2011

Dynamics of Suspended Particulate Matter in the lower Tamar estuary

Davies, E.

Davies, E. (2011) 'Dynamics of Suspended Particulate Matter in the lower Tamar estuary', The Plymouth Student Scientist, 4(1), p. 63-108.
http://hdl.handle.net/10026.1/13928

The Plymouth Student Scientist
University of Plymouth

Dynamics of Suspended Particulate Matter in the Lower Tamar Estuary

EMLYN DAVIES

Project adviser: Dr Alex Nimmo-Smith, School of Earth, Ocean and Environmental Science,
University of Plymouth, Drake Circus, Plymouth, PL4 8AA

Abstract

This project uses a combination of different measuring techniques to investigate the distribution and size of Suspended Particulate Matter within the lower reaches of the Tamar Estuary and Plymouth Sound. Data of particle concentrations and sizes, along an ebb and flood transect of the lower Tamar estuary, are presented and analysed. Expected trends of a reduction in particle concentration towards the mouth (from 7mg.L^{-1} to 5mg.L^{-1}) were detected. A decrease in particle size from 170μm furthest upstream, to 140μm near the mouth, was also observed. Significant relationships between particle size and organic concentration were found, with correlation coefficients of r = +0.5 during ebb conditions and r = +0.7 during flood conditions. Analysis of data obtained from digital holography highlighted the complex structure of flocculated particles, as well as allowing for the identification of anomalies found in LISST data. It is suggested that better shape parameterisation is required when determining particle size using LISST instruments.

Contents

List of Figures **65**

List of Tables **66**

Acknowledgements **67**

1 Introduction **68**

2 Background **69**

2.1 Estuarine Classification and Processes 69
2.2 Suspended Particulate Matter 71
2.3 Currents and Turbulence 72
2.4 Techniques & Instrumentation 74
2.5 Future Developments 76

3 Methodology **77**
3.1 Collection of Data 77
3.2 Instrumentation 79
3.2.1 1200kHz ADCP 79
3.2.2 CTD 79
3.2.3 OBS 79
3.2.4 Fluorometer 80
3.2.5 LISST-100 C 80
3.2.6 DIGIHOLOCAM 80
3.3 Filtration 81

4 Results and Discussion **84**
4.1 Salinity, Temperature & Density Structure 84
4.2 Hydrodynamics 85
4.2.1 Richardson Number 86
4.3 SPM Distribution 87
4.4 SPM Size 92
4.4.1 The Effect of Turbulence 94

5 Summary and Conclusions **98**

References **99**

Appendix **103**

A Tides **103**

B Meteorological Data **104**

C Calibration of OBS & Fluorometer **105**

D Calibration of ADCP Backscatter **107**

E ADCP Current Velocities **108**
E.1 Station Timing Check 108
E.2 ADCP Current Velocities Before Rotation 108

List of Figures

1 Sketch map of the Tamar Estuary 70
2 Station locations 77

3 Profiling frame . . . 78
4 DIGIHOLOCAM . . . 81
5 A Copepod identified from a hologram . . . 81
6 Filtration manifold set-up. . . . 82
7 Examples of filters . . . 83
8 Salinity, Temperature & Density . . . 84
9 Current velocities . . . 85
10 Richardson numbers . . . 86
11 Filtration results . . . 87
12 OBS and Fluorometer results . . . 88
13 ADCP echo amplitude . . . 89
14 Comparison between optical and acoustic backscatter . . . 89
15 Inorganic to organic ratios . . . 90
16 SPM fluxes . . . 91
17 LISST results . . . 92
18 Holograms of flocs . . . 93
19 Relationship between organic SPM concentration and particle size 93
20 Hologram of schlieren . . . 94
21 Holograms of zooplankton . . . 94
22 Kolmogorov microscales . . . 95
23 Standard deviation of particle size distribution . . . 96
24 Skewness of particle size distribution . . . 96
25 Tides . . . 103
26 Meteorological conditions preceding data collection . . . 104
27 OBS & Fluorometer calibration . . . 105
28 ADCP backscatter calibration . . . 107
29 Station timing check . . . 108
30 ADCP current velocities before rotation . . . 108

List of Tables

1 Salinity, Temperature and Density . . . 84
2 Mean concentrations of suspended particulates . . . 87

Acknowledgements

I would like to thank the following people for their assistance in the preparation of this project:

- Dr Alex Nimmo-Smith (University of Plymouth) for advice on data processing and structuring the project, and for assistance with data collection.
- Dr George Graham (University of Plymouth) for advice and assistance with data collection and processing.
- Dr Katherine Braithwaite (University of Bangor) for the processing of LISST data and assistance with data collection.
- Dr David Bowers (University of Bangor) for assistance with data collection.
- Mr Peter Ganderton (University of Plymouth) for technical preparation of the DIGIHOLOCAM and ADCP.
- Mr David Uren (University of Plymouth) for enabling the successful completion of data collection as the skipper of the research vessel.

1 Introduction

Determining the size, shape and distribution of Suspended Particulate Matter (SPM) within the water column is important for several reasons. Suspended particles affect light penetration through the water column, leading to changes in primary productivity rates (Irigoien & Castel 1997). They can also influence the way in which sound propagates through water due to reflection, affecting the performance of sonar equipment (Richards et al. 1996). The distribution of pollutants is directly affected by the distribution of SPM because many pollutants attach to the surface of particles and are therefore distributed in the same way as SPM, rather than as a dissolved substance within the water column (Gentien et al. 1995, Jackson et al. 1997, Perillo 1995). Understanding the distribution of organic carbon, (which may be in the form of Particulate Organic Carbon (POC)) and how it sinks from the atmosphere to the ocean floor, is a key stage in the carbon cycle (O'Neill 1998). This could have implications on large-scale climate prediction models. The main route by which terrestrial material is transported from land to ocean is through estuaries in the form of SPM (Perillo 1995). There are many different types of estuary, each with a wide variety of processes that affect the dynamics of SPM within the region (Perillo 1995).

This project aims to use a combination of different measuring techniques to investigate the physical processes affecting the distribution and size of SPM within the lower reaches of the Tamar Estuary and Plymouth Sound.

The project objectives are to:

- Collect accurate primary data of the following from the Tamar Estuary and Plymouth Sound:
  - Density structure
  - Current structure
  - Particle size and distribution
- Identify and explain the following physical processes affecting the distribution and size of SPM:
  - Temperature, salinity and density variation
  - Currents and turbulence
  - Flocculation
- Compare the results of particle size and distribution with that of similar studies found within the literature.

2 Background

2.1 Estuarine Classification and Processes

Estuaries can be classified in many different ways to help compare different types of environment and the processes that occur within them. The choice of classification will vary depending on the nature of the processes being investigated.

Davies (1964) created classifications based on tidal range. The following categories were used: Microtidal (tidal range less than 2m); Mesotidal (2-4m tidal range); Macrotidal (4-6m tidal range); and Hypertidal (tidal range greater than 6m). This work was extended by Nichols & Biggs (1985) to create a classification that would combine morphological and tidal effects. This resulted in three categories based on the equality between convergence (as the estuary narrows) and friction: Hypersynchronous (convergence exceeds friction, leading to an increase in tidal amplitude towards the head of the estuary); Synchronous (convergence and friction are in equilibrium with tidal forces, causing tidal amplitude to remain constant towards the head of the estuary); and Hyposynchronous (friction exceeds convergence, resulting in a decrease in tidal amplitude towards the head of the estuary).

Pritchard (1952) published classifications based solely on topography. Again, three classifications were made: coastal plain estuaries, fjords and bar-built estuaries. Davies & Hayes (1984) produced a classification that considered whether waves or tides had the greatest influence on the shoreline, which was later developed by Dalrymple et al. (1992) who related the tide, waves and river flow, giving the categories of: deltas, estuaries, strand plains and tidal flats. The need for more quantitative classifications started to develop after work by Pritchard (1955) and Cameron & Pritchard (1963), which led to three main estuarine classifications based on salinity structure: highly stratified (includes salt wedge and fjord estuaries), partially mixed and homogeneous.

Estuaries that are partially mixed (partially stratified) have a lower river flow than that of more highly stratified estuaries. Therefore, the influence of the tide is stronger so they are often classified as mesotidal according to Davies (1964). The combination of this relatively large amount of tidal energy and bottom friction, leads to a turbulent, two-layer current structure throughout the water column, with bottom friction being the dominant factor in internal mixing. As a result, mixing by both entrainment and turbulent mixing occurs. Entrainment is found in conditions where Richardson numbers exceed 0.25 (Dyer 1997). It is a one-way mixing process that causes saline water to diffuse upwards at the halocline. Turbulent mixing is a two-way mixing process at the halocline, involving breaking waves (known as Kelvin Helmholtz Billows) that occur when Richardson numbers are less than 0.25 (Dyer 1997). Salinity increases with depth and also longitudinally

towards the mouth of the estuary (Dyer 1997, Uncles et al. 1985*a*,*b*, 1986). The salinity structure often changes greatly along the length of the estuary, with more stratified water near the head, due to limited depth and increased river flow, and well mixed water near the mouth, as a result of higher velocities (Dyer 1997).

A classification system based on the relationship between the circulation parameter and the stratification parameter, that would allow a quantitative description of the types of estuary described by Cameron & Pritchard (1963), was proposed by Hansen & Rattray (1966). The circulation parameter is the ratio of the net surface current and the mean cross-sectional velocity, and the stratification parameter is the ratio of surface to bottom salinity and the cross-sectional average salinity (Hansen & Rattray 1966).

The Tamar Estuary (Figure 1) is a partially mixed and flood dominant estuary with tidal ranges of between approximately 2m and 6m (Uncles et al. 1985*a*) (This is mesotidal/macrotidal according to the Davies (1964) classification). According to the work of Grabemann et al. (1997), the total length of the estuary from Weir Head to Plymouth Sound is 31km (Figure 1) and the average river discharge is 22$m^3.s^{-1}$ (Dyer 1997).

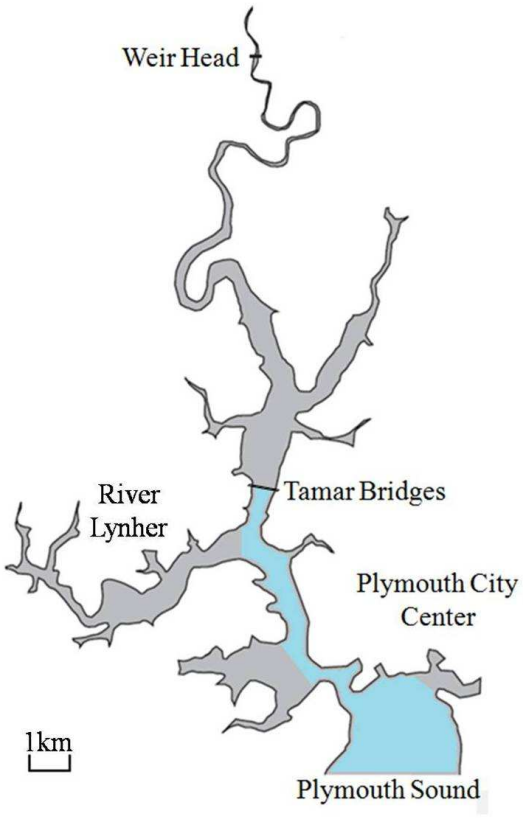

Figure 1: Sketch map of the Tamar Estuary showing the study area in blue, Weir Head at the head of the estuary, and Plymouth Sound at the mouth.
(Adapted from Grabemann et al. (1997)).

2.2 Suspended Particulate Matter

There are many different forms of SPM within the water column. They range in size from colloids (particles that are so small they are almost dissolved) of about 1μm, to organisms that could reach several metres in length (Jackson et al. 1997).

The rate at which a particle falls through the water column is determined by its settling velocity (also known as the fall velocity). Stoke's Law can be used to relate the diameter of a particle and its settling velocity, assuming spherical particles of specific sizes and densities (British-Standard 1989). Estuaries are generally regions of high velocities, and as a result, SPM concentrations are high (Perillo 1995). Small scale turbulence within the water column disrupts the passive settling of particles described by Stoke's Law (Jackson et al. 1997) and can increase settling velocities by anything up to 50% (Thorpe 2005). However, little is currently known about the structure of this small scale turbulence. It is possible to express particle size distribution by using the particle size spectrum, which describes the distribution of particles in a volume of water as a function of their sizes (Jackson et al. 1997).

The size of a suspended particle changes as other particles may become attached to one another through a processes known as flocculation, or sections may break off (floc breakup). This process of flocculation and floc breakup can occur due to a number of different reasons, including: turbulent shear, differential settling (aggregation of particles onto a floc as it falls through the water column), suspended sediment concentrations, and the presence of extra-polymeric substances (EPS) (Fugate & Friedrichs 2003, Kitchener 1972, Manning & Dyer 2002). Electrostatic charges on the surfaces of particles (Dyer & Manning 1999) and salinity (Fugate & Friedrichs 2003) are also other factors that affect flocculation, although are less likely to be influential within an estuary such as the Tamar. This is because flocculation increases with increasing salinity but reaches an equilibrium at a salinity of approximately 5-10 PSU, which is much lower than the typical salinities of between 30-35 PSU expected in the mouth of the Tamar (Uncles et al. 1986).

The majority of SPM in the open ocean is of organic origin, such as phytoplankton cells. The concentration of inorganic particles increases in nearshore regions due to discharge of clays, silts and sand from rivers (Bowers & Binding 2006, Hill et al. 2000, Perillo 1995). This would suggest that the ratio of inorganic to organic SPM would decrease from the head of an estuary to its mouth. This is likely to increase flocculation as the surfaces of organic particles have convoluted chains of sticky polymers (EPS) that, when brought into contact with another organic particle, bond together to form a larger floc. As a result, the average particle size will increase and the floc shape will become more complex (Manning & Dyer 2002). This increases the fall velocity of the particle, causing it to be more likely to

fall out of suspension. However, the density of these flocs is relatively low, leading to a decrease in the effective density (the difference between the floc density and water density) and as a result, the fall velocity is less than that of a typical inorganic particle of the same size (Dyer & Manning 1999).

There are three modes of sediment transport relevant to a study of SPM distribution in estuaries: wash load, suspension and bedload (Perillo 1995). Wash load consists of particles with a very low fall velocity, that are kept in suspension by turbulence. As a result, a vertical profile of wash load concentration is homogeneous within the regions of sufficiently high turbulence. Suspension mainly occurs as a result of erosion from the bed, when the friction velocity is approximately equal to 80% of the settling velocity. Bedload is the transport of sediment with high fall velocities, along the bed through processes such as saltation. This is often a cause of bedforms such as dunes and ripples. Sediment with grain sizes less than 150μm will be brought into suspension as soon as they start to move, whereas grain sizes greater than 150μm will be transported as bedload before moving into suspension (Perillo 1995).

2.3 Currents and Turbulence

The distribution of SPM in estuaries is affected by water motion, which is a combination of river discharge and tidal variations, as well as the smaller effects of turbulence found at boundaries within the water column (Uncles 1990). These boundary locations where turbulence is found include: the sea surface, the pycnocline, areas of high velocity shear and the bottom boundary layer. Vertical and horizontal forces are important when studying estuarine sediment dynamics. The flow of dense water beneath less dense water due to horizontal density gradients, results in vertical forces in the form of vertical gravitational circulation (Dyer 1997). The horizontal forces are in the form of tidal pumping, which is the tidally averaged transport of salt due to changes in velocity, salinity and water depth over time (Dyer 1997).

Both vertical gravitational acceleration and tidal pumping are the two main important processes in the transport of sediment in partially mixed estuaries, such as the Tamar (Allen et al. 1980, Uncles et al. 1985*b*, 1986). Uncles (1990) states that the upper reaches of the Tamar experience a net landward transport of SPM, which occurs during the flood tide. This is due to the asymmetry of the tide, which increases towards the head of the estuary to a point where river flow becomes too strong. This point is located upstream of the salt intrusion, and as a result, suspended sediment is *pumped* towards the head of the estuary. (Dyer 1997). This contributes to the formation of a turbidity maximum, which is an area of high concentrations of SPM, and is often located near the head of an estuary. In the case of the Tamar, the turbidity maximum is found in the low salinity water

near Weir Head (Figure 1). Vertical mixing increases further down the estuary causing a reduction in stratification and an exchange of particles into the lower layer, highlighting the importance of mixing on the vertical distribution of SPM (Dyer 1997, Fugate & Friedrichs 2003, Stemmann et al. 2002). At this point there is likely to be a combination of sediment being transported seaward and sediment being transported up the estuary from tidal input (Dyer 1997).

Results from Stemmann et al. (2002) and Fugate & Friedrichs (2003) have shown that the amount of mixing within the water column has an important effect on the vertical distribution of SPM. Jackson et al. (1997) suggested that this may be, in part, due to the different physical processes that affect particles of different sizes. For instance, small particles are influenced more heavily by molecular diffusion and large particles may be affected by turbulent shear. This highlights the importance of particle size and its interactions with the environment.

The Turbulent Kinetic Energy (TKE) dissipation rate (ε) is often used to characterise turbulence. It is the rate of loss of kinetic energy to heat, due to viscosity. This has an effect on the size of turbulent motions, which is expressed using the Kolmogorov microscale. The Kolmogorov microscale is the smallest size that a turbulent eddy can be before viscosity has an effect. It is a function of the TKE dissipation rate and molecular viscosity, as shown below:

$$l_K = (\nu^3/\varepsilon)^{1/4} \quad (1)$$

Where ν is the molecular kinematic viscosity. Higher TKE dissipation rates therefore lead to smaller Kolmogorov microscales (Thorpe 2005).

Fugate & Friedrichs (2003) studied the relationship between turbulence and particle size in three estuaries with different amounts of TKE, using a profiling acoustic Doppler velocimeter. It was found that surface particle dynamics were affected by irregular advection events. In mid-depth, high TKE conditions, small Kolmogorov microscales reduced particle size due to floc breakup. Stratified, low TKE regions allow differential setting to increase particle size. Suspended sediment distribution in mid-depth regions of the lower TKE areas was controlled by irregular resuspension and trapping at the pycnocline. Resuspension was the main control on suspended particle size and distribution within the bottom layers of the three estuaries.

2.4 Techniques & Instrumentation

A large range of methods have been used for determining the size and distribution of SPM. Some involve *in situ* measurements, while others require further laboratory analysis of water samples. For example, British-Standard (1989) described methods for determining particle size by passing water samples through different sized filters, then drying and weighing the filters, to determine the percentages of different particle sizes and concentrations, whereas Jackson et al. (1997) used a variety of *in situ* measurements, such as photographic camera systems and various video techniques. The fragile nature of flocs that contribute to a large proportion of SPM within estuaries, means that reliable *in situ* measurements are vital for the accurate representation of SPM dynamics (Bate & Morris 1987, Bale 1996, Eidma & Kalf 1996).

Various acoustic techniques have been reviewed by Thorne & Hanes (2002). Acoustic devices usually only measure particles down to a diameter of about 25μm and assume a spherical shape but are capable of measuring relatively large particles more accurately than most optical techniques. The Acoustic Doppler Current Profiler (ADCP), for example, is designed for measuring currents through acoustic backscatter from suspended particles, but can also give an intensity of backscatter proportional to the concentration of suspended particulate material.

Optical Backscatter Sensors (OBSs) are commonly used in determining concentrations of SPM within a water column. They measure the amount of light reflected by particles within the water column (in an arbitrary unit), which can be calibrated to give a concentration of SPM. Various errors associated with using sensors of this nature were studied by Bunt et al. (1999), and include: the shape and roughness of particles may cause significant over-estimations of particle size; particle flocculation and air bubbles may increase the response of the OBS by up to two times; plankton may increase the response of the OBS by four times.

Bale (1996) and Agrawal & Pottsmith (2000) described the way in which a LISST (Laser *In Situ* Scattering Transmissometer) uses the principles of laser diffraction to measure particles. The instrument is set up so collimated laser light passes through the sample volume onto a receiving lens. A specially made detector, positioned at the focal plane of the receiving lens, receives a focused diffraction pattern caused by small particles within the sample volume. The angle at which a ray is diffracted by these small particles is proportional to the radius of its diffraction pattern on the detector. This radius increases logarithmically as the diffraction angle increases. The optical power distribution on the ring detector gives the essential information on particle size distribution within the sample volume. For example, large particles cause a peak in optical power at small angles. The inversion of power distribution sensed by the rings produces an area distribution of particles. The volume distribution of particles is obtained from the

area distribution, by multiplying the area in any size class by the median diameter in that size class. The total volume concentration in the sample can then be obtained by summing the volume distribution. One disadvantage of this technique is that it assumes spherical particles when calculating sizes (Lynch et al. 1994), which could lead to significant errors as most organic SPM is very variable in shape and form. A study by Mikkelsen et al. (2005) compared the use of LISST instruments with a particle imaging system and found that the LISST had a tendency to underestimate sizes. The application of *in situ* measurements made by LISST instruments and other laser techniques in estuaries has been investigated in a number of studies, including those of Bate & Morris (1987) and Law. et al. (1997).

Schlieren is a phenomenon that occurs due to a combination of strong density gradients and turbulence that cause changes in the refractive index of a fluid (Mikkelesen et al. 2008). This has proved to be a problem when using many of the light-dependent, *in situ* techniques described above. A number of studies have reviewed the effect of density stratification on the performance of LISST instruments, and concluded that density stratification produces similar results to areas of high particle concentration (Mikkelesen et al. 2008, Styles 2006). Systems that measure particle characteristics from images also encounter the same problems. However, the areas in which schlieren has significant influence can be identified, and the associated measurements can be discarded.

A number of recent techniques that collect images of particles *in situ*, have been used to try and quantify accurate SPM characteristics. For instance, the *In Situ* Particle Imaging Device (InSiPID) uses CCD video cameras and digital image processing algorithms to measure particle size and shape (Benson & French 2007). Other studies that evaluate the use of camera systems for measuring SPM include that of: Dyer et al. (1996), Eidma & Kalf (1996), Knowles & Wells (1996), Maldiney & Mouchel (1996), Milligan (1996), VanLeussen & Cornelisse (1996) and Syvitski & Hutton (1996).

2.5 Future Developments

A vast amount of research has been conducted on the sediment dynamics that relate to the turbidity maximum within specific estuaries (which are often located towards the upper limit of the salt intrusion), as well as sediment fluxes of organic and inorganic particles between oceans and estuaries. However, little is known about the sediment fluxes of particles of different shapes and the relationship between particle shape and composition. This could be of vital importance when modelling the distribution of pollutants if, for instance, a specific pollutant was only found on particles with specific characteristics.

Turbulence has been studied in great detail at various important locations such as the bottom boundary layer and strong density interfaces. The relationship between suspended particle dynamics and turbulence has been a recent area of study. However, there is a lack of knowledge on the exact relationship between the Kolmogorov microscale and suspended particle dynamics.

The techniques used for measuring particle size and concentration are varied, each with their own associated errors. The effect of schlieren on the reliability of optical instruments has been identified and led to the development of instruments that measure particles through the use of images. The effect of particle shape on sediment dynamics has had little attention within the literature, and may be of significant importance because of the difference in characteristics between organic particles and inorganic particles. The reason for this is likely to be due to the lack of resolution of current instrumentation and that there appears to be no instrument that is capable of measuring particle characteristics in three dimensions.

3 Methodology

3.1 Collection of Data

Ebb and flood transects of the Tamar Estuary and Plymouth Sound were surveyed on 19/06/08. The transect started with Station 1 at the area of The Tamar Bridges and finished close to Duke Rock, near the Eastern entrance of Plymouth Sound. It consisted of 15 sample stations, approximately 0.5km apart, as shown in Figure 2. The exact distance between stations varied slightly due to hazards such as Devonport dockyard and chain ferries. The chosen positioning of the transect was determined by studying the tidal stream atlas of Plymouth Sound (Admiralty n.d.). It followed the strongest tidal flows through Plymouth Sound and The River Tamar. For tidal heights and times at each station see Figure 25 in Appendix A.

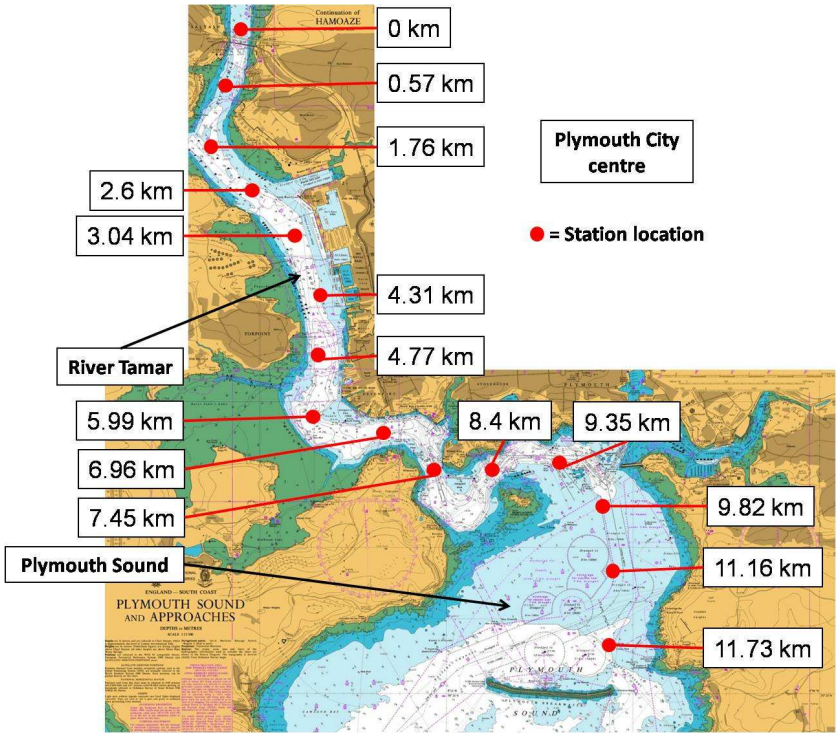

Figure 2: Admiralty chart showing the locations of each station along the transect.

At each station the following samples were taken:

- CTD profile - (conductivity and temperature - allowing the calculation of water density)
- DIGIHOLOCAM (Digital In-line Holographic Particle Imager) profile - (particle size, shape and concentration)
- LISST-100 C profile - (particle size distribution)
- OBS (optical backscatter) profile - (particle concentration)

- Fluorometer profile - (chlorophyll concentration)
- Surface water sample - (concentrations of organic and inorganic particles)

The CTD, Fluorometer, OBS, LISTT-100 C, and DIGIHOLOCAM were attached onto a single frame (Figure 3) to allow the sensors to be as close to each other as possible in order for them to be recording within the same area. The maximum depth of each profile was approximately 1m above the bed.

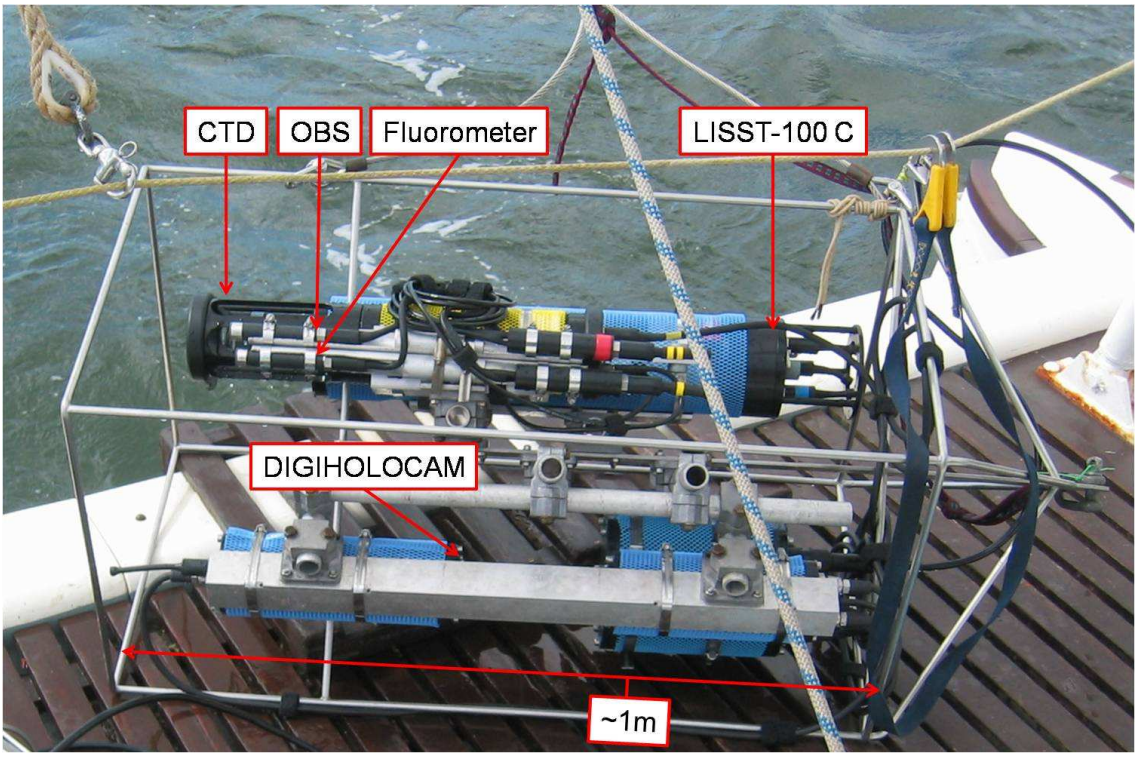

Figure 3: CTD, OBS, Fluorometer, LISST-100 C and DIGIHOLOCAM on the profiling frame.

Three surface water samples were taken at each site to allow calibration of optical and acoustic backscatter instruments. Ideally, repeats of ebb and flood transects over a number of days or months would have allowed the data to be tidally averaged. However, this was not possible due to the time that the equipment was available for. It would have been beneficial to take water samples at the surface, mid-depth and near the sea bed. However, the boat used did not have the capacity to carry the amount of water that would have been collected.

A ship-mounted 1200kHz ADCP was running continually to record current velocity and acoustic backscatter intensity. This allowed relationships between current flows, turbulence and the distribution of suspended particles to be examined, as well as a comparison between acoustic and optical backscatter.

The filtration of the water samples was carried out using standard filtration methods, as described in section 3.3.

3.2 Instrumentation

3.2.1 1200kHz ADCP

The ADCP (Acoustic Doppler Current Profiler) produces an instantaneous velocity profile of the water column, which can then be presented in a graphical form to allow analysis of the current features measured. TKE dissipation can also be calculated using a structure function technique proposed by Wiles et al. (2006), to allow a comparison between particle characteristics and turbulence.

The ADCP emits pulses of sound from a number of transducers on the instrument (usually 4). The sound pulses are then reflected off scatterers in the water column, allowing the speed of the scatterer to be calculated. It is, however, assumed that the scatterers used to calculate current speeds move at the same speed as the water.

During the transect of the Tamar the movement of the boat over ground was removed from the initial velocities recorded by the ADCP, through bottom-tracking.

Possible sources of error can occur in rough weather if the transducers are too close to the water surface because a large amount of bubbles are created by breaking waves. This increases the backscatter from the ADCP and produces noisy data in the surface layer. Also, there is often a decrease in accuracy near bottom of the profile due to the high reflectivity of the bed. In order to compensate for these two errors, the ADCP was positioned at a depth where there would be minimal interference from surface bubbles but also as close to the surface as possible, and the lowermost layer of the profile was removed. The ADCP was also changed from mode 12 to 1 during rougher conditions to compensate for greater boat movements from waves.

3.2.2 CTD

A CTD measures conductivity, temperature and pressure. Salinity was calculated from conductivity and temperature, allowing density to then be calculated with salinity and temperature.

3.2.3 OBS

The OBS (Optical Backscatter) sensor measures the amount of backscatter from all particulate matter within the water column. This allows a comparison between the optical backscatter and the concentration of total suspended solids (TSS) obtained from the filtration of surface water samples (Section 3.3). This then allows for the response from the OBS to be calibrated to give the associated concentration of SPM in $mg.L^{-1}$, as shown in Appendix C.

The main error associated with OBS sensors is that anything within the water that scatters light (e.g. a bubble of air) will be recorded as a particle, in a similar

way to the ADCP.

3.2.4 Fluorometer

The Fluorometer measures fluorescence from particles containing chlorophyll - a. Again this can be calibrated against the filtration of surface water sample (Section 3.3) to give an indication of the concentration of particulate organic matter (Appendix C). However, there are discrepancies associated with this comparison as not everything that combusts during the filtration process will also fluoresce.

3.2.5 LISST-100 C

LISST (Laser In Situ Scattering and Transmissometry) sensors measure particle size and concentration using the principles of laser diffraction (Agrawal & Pottsmith 2000). This is the principle that as collimated light is shone through a sample volume containing particles, the light will diffract around each particle at an angle that is proportional to the size of the particle. After being passed through a focussing lens, these diffraction patterns are focused onto a ring detector. Light intensities at specific locations on the ring detector are therefore proportional to the concentration of particles of a certain size.

The LISST assumes that all particles in the sample volume are near-spherical. It has also been suggested that LISST instruments are not reliable when under the influence of schlieren, which is a phenomenon caused by density differences within the water causing light scattering (Mikkelesen et al. 2008).

3.2.6 DIGIHOLOCAM

The DIGIHOLOCAM (Digital In-line Holographic Particle Imager) (Figure 4) uses the same principles of laser diffraction as the LISST but the ring detector and focussing lens in the LISST are replaced by a video camera that records holographic images. The holographic images can be digitally analysed to identify the size and shape of individual particles within the sample volume.

One of the advantages of using digital holography to examine particles is that possible causes of anomalies can be identified from the images. For example, a Copepod may appear as an unusually large particle and would not be able to be identifiable by instruments such as a LISST. It could, however, be identified clearly on a hologram, as shown in Figure 5.

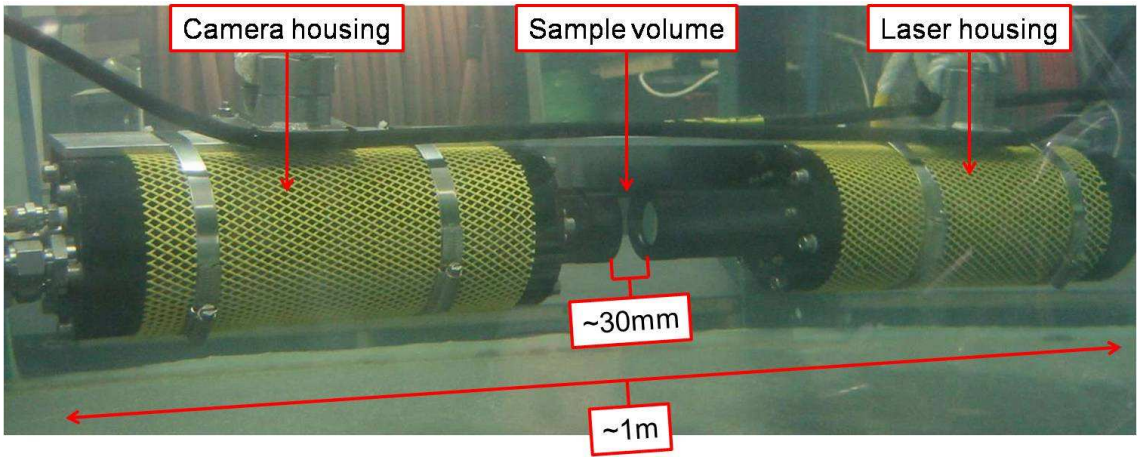

Figure 4: The DIGIHOLOCAM in a laboratory test tank. (Nimmo-Smith 2008)

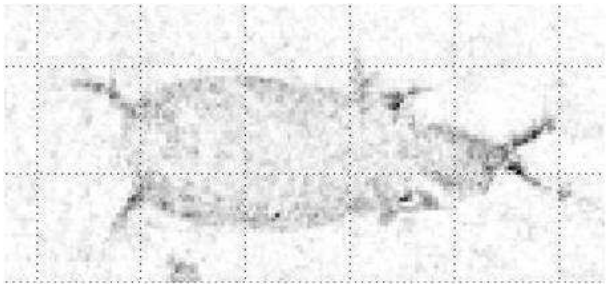

Figure 5: A Copepod identified from a hologram. Grid spacing = 0.2mm. (Nimmo-Smith 2008)

3.3 Filtration

The filtration of surface water samples was carried out using the standard filtration techniques described in this section.

In order to avoid contamination, forceps were used to handle filters and each filter was stored in a clean packet for transportation and heating.

1. Filter preparation:
   Each filter was rinsed three times with 50ml of Milli-Q water and combusted at 450^{o}C for 4hours. The filters were then weighed using an analytical balance.

2. Water sample collection:
   There were two approaches taken to this aspect of the method. Three surface water samples were collected at each station and stored in bottles for filtration the following day for Method A. Filtration was carried out three times for each water sample and the sample bottles were kept cool to reduce growth of organic matter. Method B consisted of only one filtration per sample but was carried out immediately after the sample was collected.

3. Filtration:
   50ml of Milli-Q water was past through the filter to allow the filter to stick to the frit (Figure 6) before a known amount of sampled water was filtered (approximately 1 litre). The filter was then rinsed a further 3 times with 50ml of Milli-Q to wash any remaining water sample through the filter.

4. Total suspended solids:
   After filtration the filters were dried at 80^{o}C for 16hours and weighed. The difference in weight between the dried filter and the initial filter weight was divided by the amount of water sample filtered and multiplied by 1000 to produce a result in mg.L^{-1}.

5. Organic matter:
   The filters were then combusted at 450^{o}C for 4hours in order to remove any organic matter on the filter. The filters were re-weighed to allow the concentration of organic matter (in mg.L^{-1}) to be calculated from the difference in weight between the dried and combusted filters.

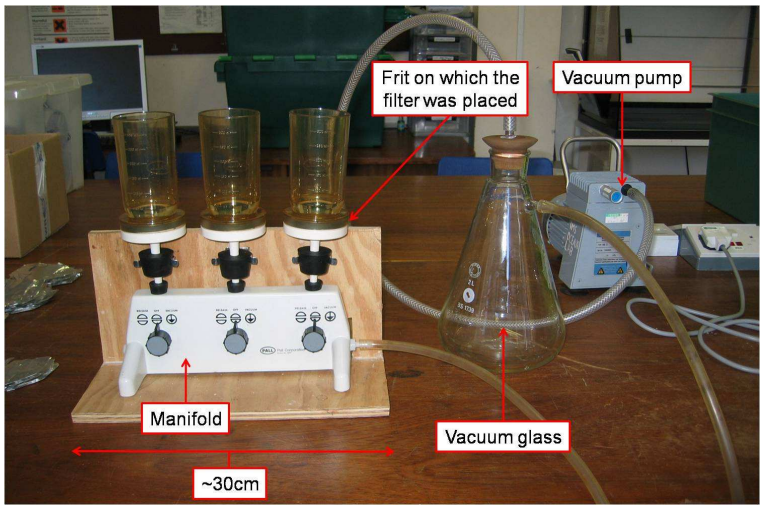

Figure 6: Filtration manifold set-up.

Figure 7 shows the colour change of the filters after each stage of filtration. The combustion process resulted in a change from green to brown, which can be seen when comparing Figures (b) & (c). This is due to the green colours associated with organic substances being burned during the combustion process, leaving the brown colour of the inorganics to be left on the filter. As the same volume of water sample was passed through all the filters shown in Figure 7, It is clear from the intensity of colour on each filter, that a larger concentration of SPM was present on the filters on the right compared with those on the left.

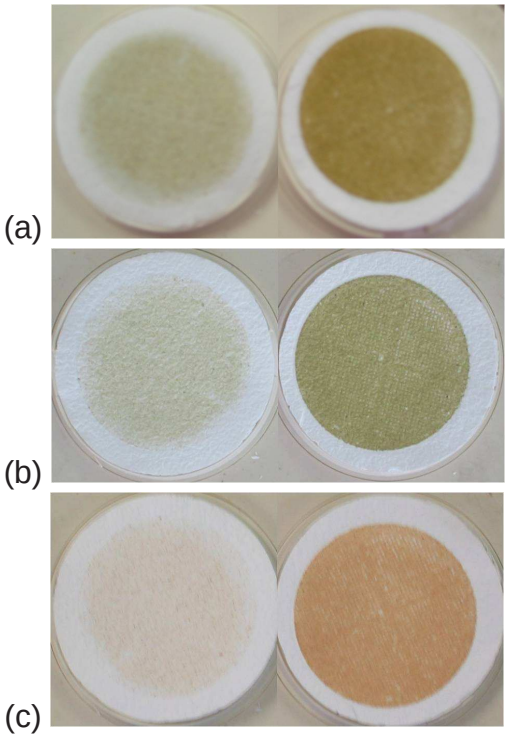

Figure 7: (a) Filters before drying. (b) Dried filters. (c) Combusted filters. The filters on the left were from Station 15 (Plymouth Sound) and the filters on the right were from Station 1 (Tamar Bridges) (see Figure 2).

4 Results and Discussion

4.1 Salinity, Temperature & Density Structure

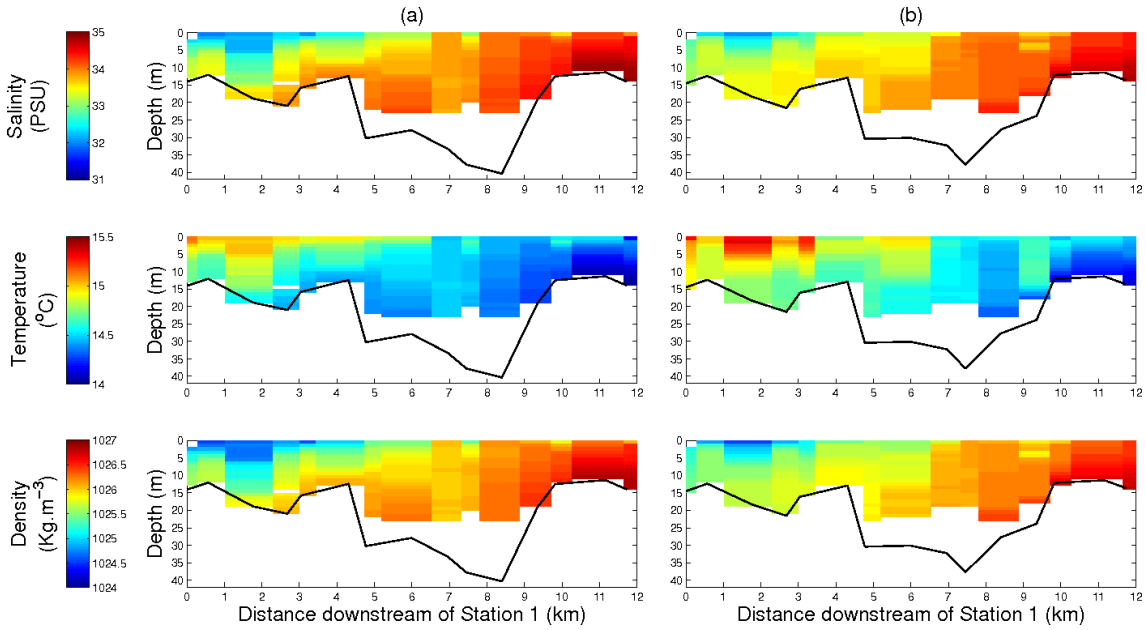

Figure 8: Distributions of temperature, salinity and density along the ebb (a) and flood (b) transects.

Table 1: Summary of mean salinities, temperatures and densities.

	Ebb	Flood	Tidally-averaged
Mean Salinity (PSU)	33.72	33.72	33.72
Mean Temperature (°C)	14.5	14.7	14.6
Mean Density (kg.m^{-3})	1025.9	1025.9	1025.9

Figure 8 and Table 1 show that salinity increased towards the mouth and with depth. The flood tide caused an increase in salinity towards the mouth but did not change the mean salinity of the transect because the range of salinities decreased.

Temperature decreased with depth and towards the mouth. The mean temperature was lower during the ebb transect. Temperature in the surface layers and upper half of the transect are greater on the flood tide. This is likely to be as a result of an increase in air temperature over time because the flood transect was carried out in the afternoon.

Salinity had a greater effect on density than temperature and, as a result, density followed a similar pattern to that of salinity. There are some areas where temperature does cause differences, for example, the high temperatures between 1 and 2km downstream of station 1 in the flood transect.

These results are characteristic of a typical partially mixed estuary described by Dyer (1997) & Uncles et al. (1986).

4.2 Hydrodynamics

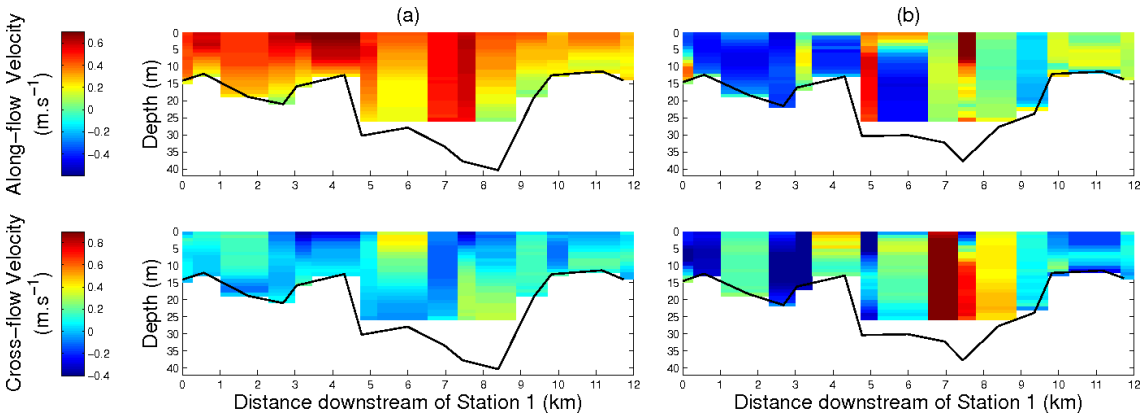

Figure 9: ADCP current velocities recorded on the ebb (a) and flood (b) transects. Positive along-flow velocities indicate current flowing in-line with the river flow (i.e. from source to mouth). Positive cross-flow velocities indicate current flowing at 90° to the right of the river flow and negative velocities correspond to current flowing at 90° to the left. Current directions shown are rotated to be in-line with the depth contours in the area of each station and the velocities were averaged over the time spent at each station (Appendix E).

Along-flow currents were faster in the ebb transect, with a mean flow of 0.37 m.s^{-1} compared to the -0.03 m.s^{-1} mean flow in the flood transect. Reduced velocities can be seen in areas near the bed (black line), for example in the ebb transect between 2 and 3km from Station 1. Faster cross-flowing currents were present in the flood transect as well as larger deviations in current direction from the orientation of the estuary channel. This is likely to be due to the sinuosity and convoluted shape of the estuary channel. The high positive cross-flow velocities between 5 and 7 km downstream of Station 1 during the flood transect are likely to be due to the inflowing water filling the tidal lake to the west of the stations in the area. Larger fluctuations in current speed were also present during the flood transect. The tidally-averaged velocity for the area was +0.17m.s^{-1}, suggesting ebb dominant flows.

The area known as “the narrows” is situated between 7.5 and 8km downstream of Station 1 (Figure 2). This is a narrow channel that effectively creates a bottleneck in the estuary. Here, strong along-flow currents were recorded during the ebb transect. During flood conditions, very fast surface flows and near-stationary flows in the lower half of the water column were recorded in the direction of the channel (along-flow). In the area of the water column where the slow along-flows were recorded there were high positive cross-flows. This suggests that the water flowing from west to east around the North of Drake’s Island (Figure 2) had not been substantially influenced by the topography surrounding the area. This may be because of the much deeper water shown by the ADCP bottom tracking (black line on Figure 9).

4.2.1 Richardson Number

The Richardson number is a measure of the type of mixing within the water column. It is a function of the ratio of density stratification to velocity shear and was calculated using the following formula:

$$Ri = -\frac{g}{\rho}\frac{\partial \rho}{\partial z}/(\frac{\partial u}{\partial z})^2 \quad (2)$$

For Richardson numbers (Ri) above 0 the stratification is stable. Here, either entrainment or turbulent mixing may be present. Entrainment results in the upward transport of dense water due to waves breaking at the pycnocline and is found when $Ri >$ 0.25. Turbulent mixing occurs between Richardson numbers of 0 and 0.25. This type of mixing is characteristic of a more balanced exchange where both dense water is lifted and less dense water is brought down. When $Ri <$ 0 unstable water is present, where dense water overlies less dense water (Dyer 1997).

The calculated Richardson numbers shown in Figure 10 indicate more areas of instability and turbulent mixing during the flood transect. Most of this is found between 5 and 8km downstream of Station 1, which coincides with areas of large gradients in current velocity (Figure 9). These areas of more mixing could have resulted in increased particle collisions that would increase flocculation and hence, particle size. However, increased mixing may also have caused an increase in velocity shear across individual particles, leading to floc break up. As a result, no relationship was found between particle size and Richardson number.

The relatively shallow profiles of Station 10 (7.5km downstream of Station 1), present in both transects shown in Figure 10, are due to high current volecities (Figure 9) causing the line holding the instruments to stream behind the survey boat.

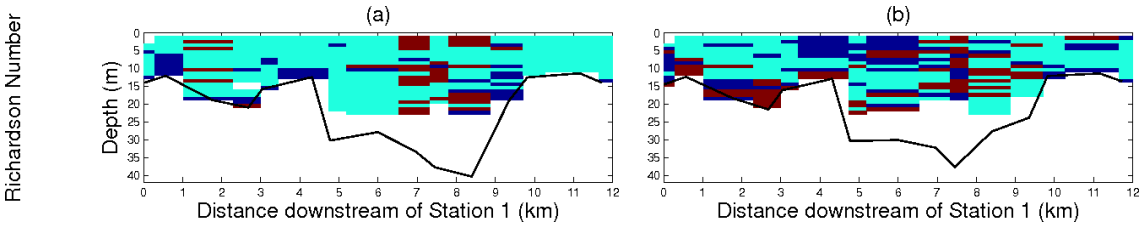

Figure 10: Richardson numbers of the ebb (a) and flood (b) transects. Red indicates unstable water ($Ri <$ 0). Blue colours indicate a stable water column ($Ri >$ 0), with light blue being conditions of entrainment ($Ri >$ 0.25) and dark blue being conditions of turbulent mixing (Ri = 0-0.25).

4.3 SPM Distribution

The results from the filtration of surface water samples show a decrease in both organic and inorganic SPM towards the mouth of the estuary during ebb and flood conditions (Figure 11). There was a greater decrease in concentration towards the mouth during the flood transect. The mean concentration of SPM only changed by 0.1mg.L^{-1} from the ebb to flood transects. However, the relative amounts of inorganic and organic SPM were markedly different in the two transects (Table 2).

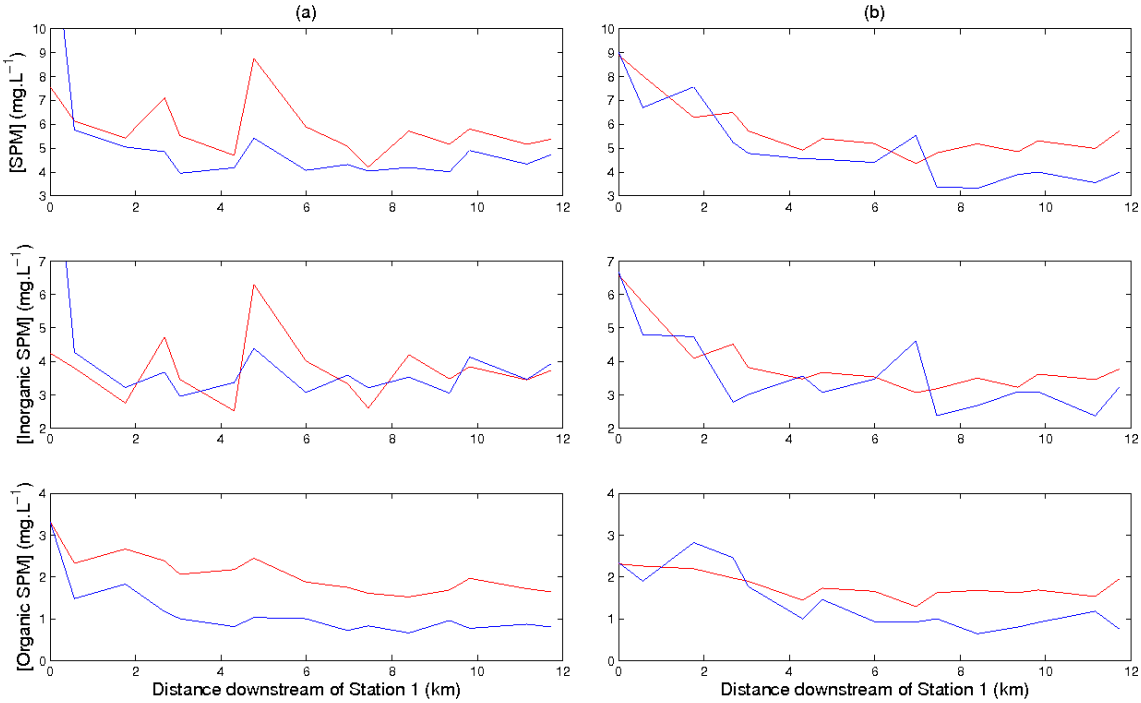

Figure 11: Concentrations of suspended particulates obtained from the filtration of surface water samples during the ebb (a) and flood (b) transect. Red lines are concentrations obtained from Method A (three repeats of filtration, as shown in section 3.3) and the blue lines show concentrations from Method B (one repeat carried out immediately after the water sample was taken). Error bars are not shown to allow for easier interpretation.

Table 2: Mean concentrations of suspended particulates for each transect. Using the method described in section 3.3.

	Ebb Transect		**Flood Transect**	
(Concentrations in mg.L^{-1})	Method A	Method B	Method A	Method B
Mean [SPM]	5.8	5.3	5.7	5.0
Mean [Inorganic SPM]	3.8	4.1	4.0	3.6
Mean [Organic SPM]	2.1	1.2	1.8	1.4

The concentrations of SPM obtained from filtration that are presented in Figure 11, show a decrease in the concentration of organic particles towards the mouth. The results of the filtration using the method described in section 3.3 (Method A - red lines) gave consistently higher concentrations of organics than those obtained

from filtration immediately after the water sample was collected (Method B - blue lines). This is likely to be due to growth of organic material in the water sample between the time of collection and filtration. The differences between the two techniques, however, was within the confidence level of the results and therefore could have been due to chance.

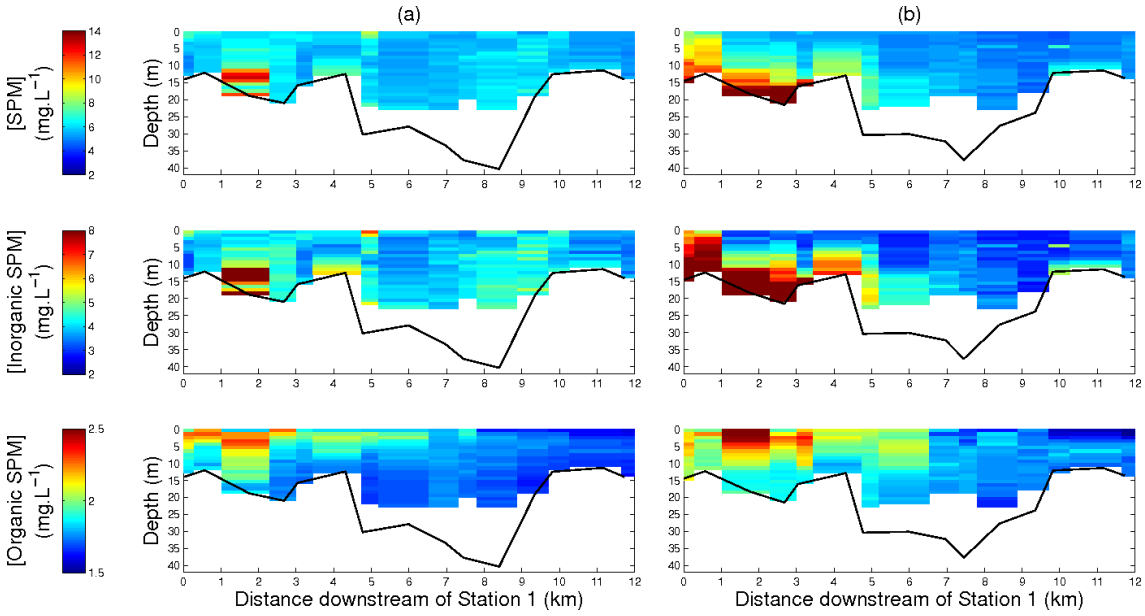

Figure 12: Concentrations of SPM (obtained from the OBS), inorganic SPM and organic SPM (obtained from the Fluorometer) along the ebb (a) and flood (b) transects.

Figure 12, which displays the distribution of SPM along the two transects, shows that the greatest concentrations of SPM (10-14mg.L^{-1}) were in the lower layers of the flood transect between 0 and 4km downstream of Station 1. The majority of these particles were inorganic. High concentrations of organic particles ($>$2.5mg.L^{-1}) were found in surface waters between 0 and 6.5km downstream of Station 1.

An indication of relative changes in SPM concentration were also estimated using acoustic backscatter from the ADCP (Figure 13). This correlates well with the concentration of SPM obtained from the OBS (Figure 12 and 14). However, there are a number of discrepancies, for example between 7 and 8 km downstream of Station 1 during the flood transect. This coincides with an area of high velocities (Figure 9) which may have resulted in an increase in the number of bubbles in the water column, causing an increase the amount of backscatter. This is supported by a larger spread of ADCP echo amplitudes at the locations of low OBS backscatter, as shown in Figure 14. This suggests that the ADCP was responsive to more scatterers within the water column than the OBS. However, there was no significant relationship between the ADCP echo amplitude at a depth of 2m and the concentration of SPM obtained from filtration (see Appendix D). This suggests that the the ADCP was responding to scatterers other than SPM, for example bubbles created by surface waves. The backscatter from

the ADCP was therefore not calibrated from the filtration results and is instead presented with a scale of low to high intensities.

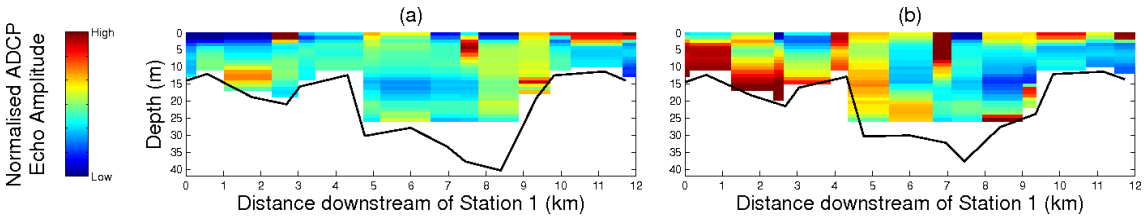

Figure 13: Normalised echo amplitudes obtained from the ADCP along the ebb (a) and flood (b) transects.

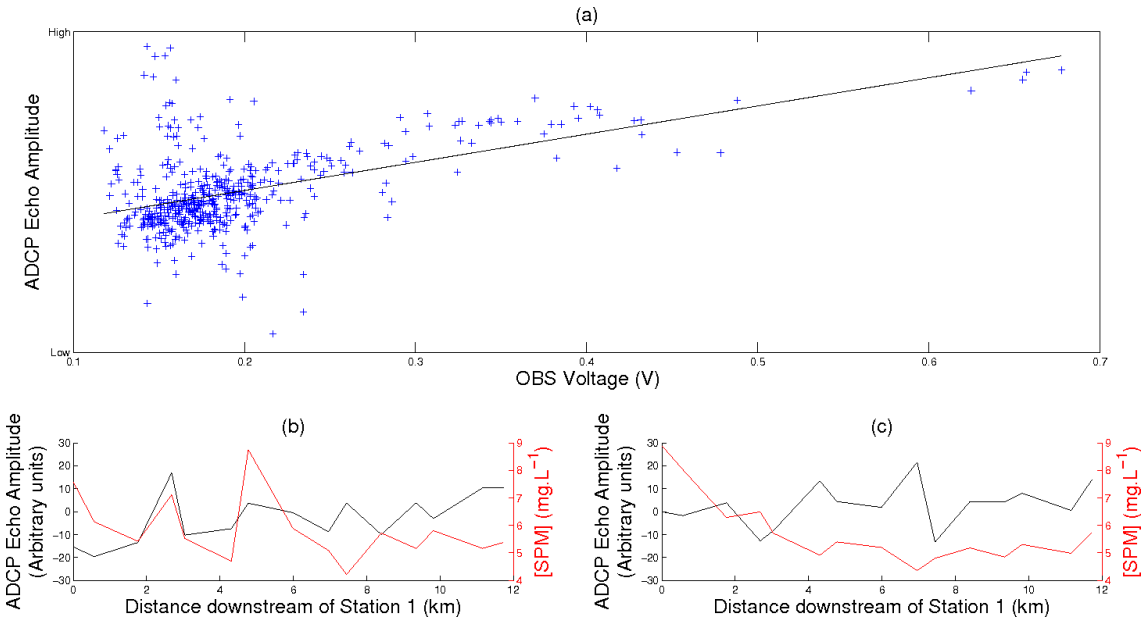

Figure 14: (a) The relationship between echo amplitude from the ADCP and the OBS response. This relationship is significant, with a correlation coefficient of +0.5, as the minimum coefficient required at 0.05 level of significance is 0.098. ADCP echo amplitudes at a depth of 2m and the SPM concentrations obtained through filtration are also shown from the ebb (b) and flood (c) transects.

The coloured plots of Figure 15 show large vertical gradients in the ratio of inorganic to organic SPM between 0 and 6 km from Station 1 during the flood transect. This is due to a high concentration of organics near the surface overlying a high concentration of inorganics near the bed (Figure 12). As discussed earlier, this is likely to be as a result of a greater light intensity and temperature near the surface.

The line graphs show no significant change in the ratio of inorganic to organic SPM towards the mouth during the ebb transect, whereas a strong negative correlation was found in the flood transect (Figure 15). This may be due to the differences in the time at which the data were collected as the first stations of the ebb transect were recorded in the first hour of the tidal cycle. This was soon after slack water, where the tidal currents were relatively weak. However, during the

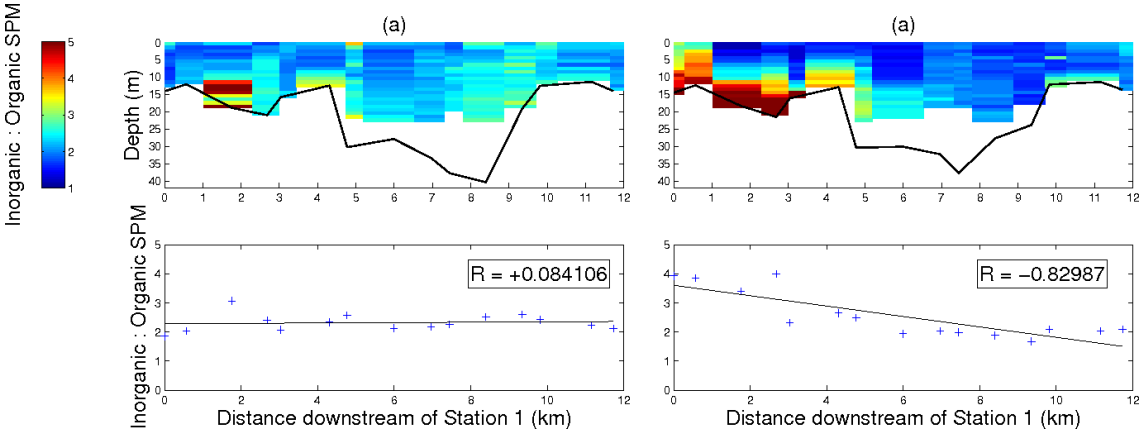

Figure 15: Ratios of inorganic to organic SPM along the ebb (a) and flood (b) transect presented as coloured surface plots of bin-averaged values (top) and a line graph of mean values at each station (bottom). As the ratio increases, the relative amount of inorganic SPM increases. (Minimum correlation coefficient required at 0.05 level of significance = 0.482.)

flood transect, data from these stations were collected in the last hour of the tidal cycle. This was relatively soon after the area had been subjected to the stronger flows of the third and fourth hour of the flood tide, as shown between 5 and 8km downstream of Station 1 in Figure 9 (b). The resultant increases in mixing were observed in these highly concentrated areas of the lower layers of the flood transect, as expected (Figure 10). This increase in mixing would then allow more sediment in the bed layer to be brought into suspension. The diffusion processes associated with this mixing are then likely to decrease the sediment concentration gradient, effectively lifting the regions of high concentration up the water column. As a result, an increase in concentration of inorganic SPM was observed within these areas of the flood transect (Figure 12). It would also be expected that there would be an increase in particle size as more sediment is brought into suspension through these higher current velocities. This is supported by the stronger relationship between particle size and distance from the head of the estuary during the flood transect (Figure 17).

As the majority of the SPM in the open ocean is of organic content, such as phytoplankton, the overall increase in the relative concentration of organic SPM towards the mouth during the flood transect is as expected and is supported by the work of Bowers & Binding (2006), Hill et al. (2000) & Perillo (1995).

The fluxes of SPM shown in Figure 16 indicate little movement of sediment in Plymouth Sound (between 8 and 12km) during the start of the flood tide. The greatest movement occurred in the upper 5km of the flood transect. This is likely to be due to the high concentrations of sediment recorded at this time (Figure 12) rather than high current velocities (Figure 9).

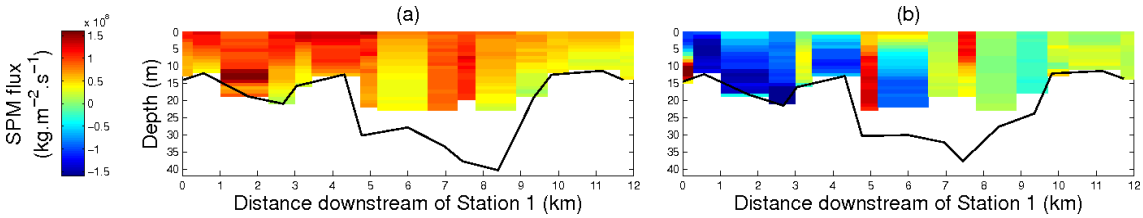

Figure 16: SPM Fluxes for the ebb (a) and flood (b) transects. The fluxes shown were calculated by multiplying the concentrations of total SPM by the along-flow velocity. This assumes that suspended particles within the water column move at the same rate as the water, and as a result the fluxes shown will be slightly overestimated.

4.4 SPM Size

There were large fluctuations in mean particle size throughout both ebb and flood transects, as shown by the coloured plots of Figure 17. However, a statistically significant decrease in depth-averaged mean particle size towards the mouth was found during both ebb and flood conditions. It would be expected that particle size would increase with depth due to lower fall velocities of smaller particles. However, there was no correlation between mean particle size and depth. An explanation for this may be that current velocities throughout the water column were greater than the threshold required to keep particles in suspension.

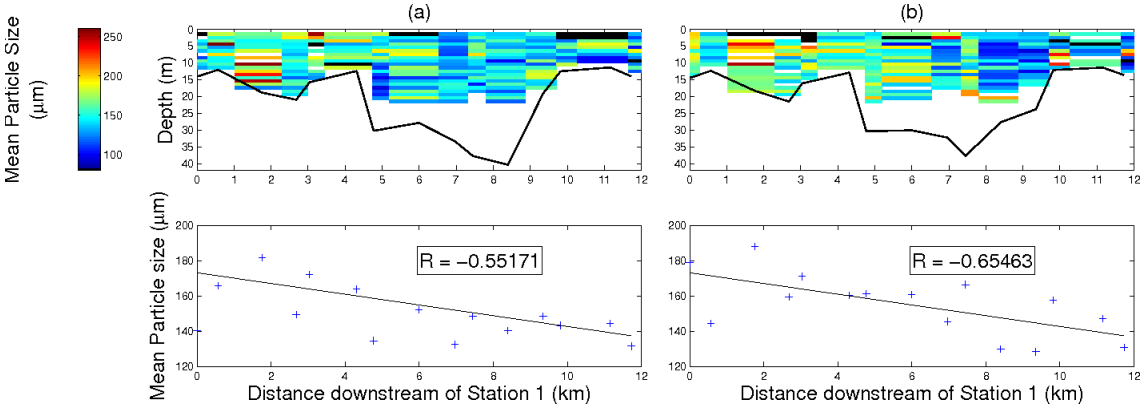

Figure 17: Mean particle size for each depth bin along the ebb (a) and flood (b) transects obtained from the LISST. The coloured plots (top) show mean sizes in 1m depth bins along the transect. The line graphs (bottom) show mean particle sizes for each station. Black data cells are areas that have been discarded due to schlieren. (Minimum correlation coefficient required at 0.05 level of significance = 0.482.)

The decrease in size towards the mouth shown in Figure 17 can be explained by a decrease in the concentration of organic SPM (Figure 12). There are two possible reasons for this: either more organisms such as plankton were situated further towards the head of the estuary or there were larger flocs dominating the area. The reason for larger flocs in areas of high organic SPM concentration is that the surfaces of an organic particles consist of convoluted polymer chains, known as EPS (extra-cellular polymeric substances), which increase the strength of the bond between flocculated particles (Manning & Dyer 2002). When combined with turbulent flows that increase particle collisions, this phenomenon increases flocculation, and hence an increase in particle size was observed. The flocs that result have a relatively low density as the EPS allow particles to be bonded together with relatively large spaces between the particles that make up the floc. This decreases the effective density, resulting in the fall velocity of the floc being less than that of a typical inorganic particle of the same size (Dyer & Manning 1999). Analysis of images obtained from the DIGIHOLOCAM supported this (Figure 18), emphasising the importance of EPS to flocculation, as highlighted by Kitchener (1972). It is likely that the size of these particles were

underestimated by the LISST, as each cluster of solid material would have been considered as an individual particle. In spite of this error, a statistically significant relationship between the concentration of organic material and the mean particle size was found using particle size data obtained from the LISST (Figure 19). This correlation was stronger during the flood transect, which may be explained by a greater amount of mixing during the flood tide (Figure 10), causing an increase in particle collisions and therefore a greater chance of flocculation.

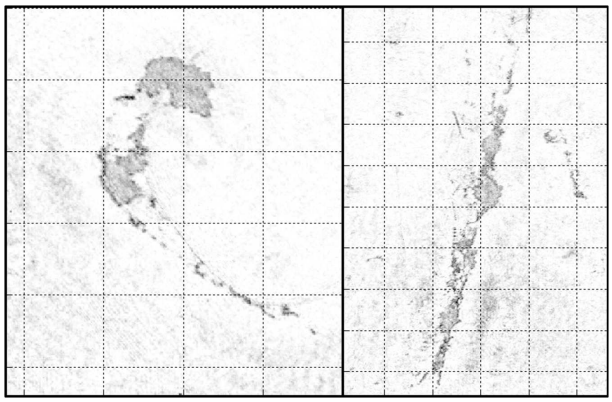

Figure 18: Examples of flocs recorded by the DIGIHOLOCAM. Individual clusters of solid material joined by EPS are clearly visible. (Grid spacing = 0.5mm.)

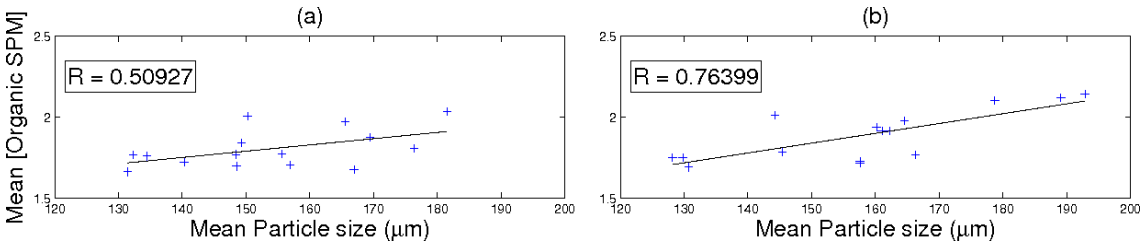

Figure 19: Relationship between concentration of organic SPM and mean particle size for the ebb (a) and flood (b) transects. (Minimum correlation coefficient required at 0.05 level of significance = 0.482.)

A number of anomalies were identified in the LISST data and presented as black data cells in Figure 17. Most of the anomalous data points were in the upper 4m of the water column and were identified as schlieren using the DIGI-HOLOCAM. This was found to cause distortions in the images that prevented any calculation of particle size, shape or concentration (Figure 20). In these areas the LISST produced anomalous peaks in particle size, and as a result, the data from these locations were discarded. The work of Mikkelesen et al. (2008), contradict this, suggesting that schlieren causes an apparent decrease in particle sizes identified by the LISST. The removal of schlieren-influenced data resulted in a 2% decrease in the overall mean particle size estimated by the LISST.

Other possible anomalies highlighted by the DIGIHOLOCAM were that of zooplankton such as crustaceans, as shown in Figure 21. However, the distribution of these organisms was so sparse that their effect was negligible.

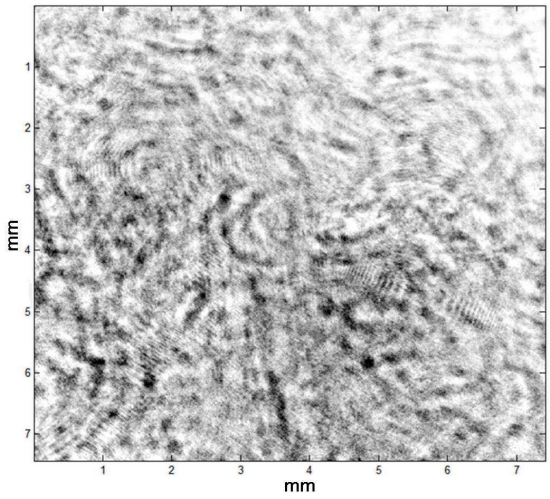

Figure 20: Raw DIGIHOLOCAM image of schlieren at a depth of 2.6m at station 8 (6km downstream of Station 1) of the flood transect.

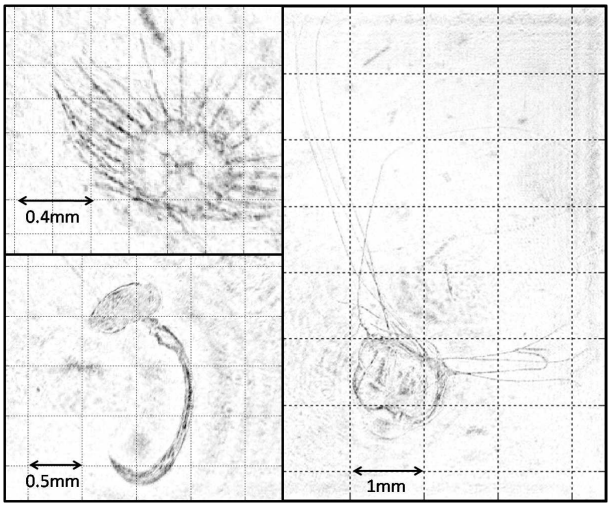

Figure 21: A selection of holographic images of zooplankton recorded by the DIGI-HOLOCAM.

4.4.1 The Effect of Turbulence

The structure function technique proposed by Wiles et al. (2006) was used to calculate TKE dissipation from the individual velocity beams of the ADCP. Equation 1 was then used to calculate the associated Kolmogorov microscale.

It would be expected that turbulence would act to both increase the size of small particles by increasing collisions and hence flocculation, and to decrease the size of large particles due to velocity shear across the diameter of the particle, causing floc breakup (Fugate & Friedrichs 2003). This would suggest that a decrease in Kolmogorov microscales would result in a smaller mean particle size and a reduction in the standard deviation of the particle size distribution. However, there was no significant correlation between mean particle size and the Kolmogorov microscale (Figure 22) or the standard deviation of particle size distribution and the Kolmogorov microscale (Figure 23). It would also be expected

for the skewness of particle size distribution to be affected by turbulence. The skewness is a measure of the asymmetry of the data around the mean. A negative skewness indicates that the distribution is spread out more to the left of the mean, with a peak to the right. A positive skewness indicates a spread to the right, with a peak to the left of the mean. It would therefore be expected for larger Kolmogorov microscales to allow for larger particles and therefore a smaller skewness and for small Kolmogorov microscale to be associated with larger skewness values. However, there was no significant relationship found between Kolmogorov microscales and skewness, as shown in Figure 24.

There are a number of possible explanations for finding no significant relationships between Kolmogorov microscale and the particle size distribution. Firstly, a turbulent eddy is likely to reduce the size of larger particles, and will therefore not have a strong relationship with the mean particle size. It may therefore be more beneficial to investigate the relationship between Kolmogorov microscale and maximum particle size or the skewness of the particle size distribution. Another explanation may be that the area of data collection was not a region of high TKE, leading to biological processes such as bonding through EPS to play a greater role in the flocculation process due to observed Kolmogorov microscales being too large to cause floc break up (Figure 22 (c)). Also, differential settling is likely to play a greater role in flocculation in lower TKE conditions (Fugate & Friedrichs 2003). This would therefore lead to the conclusion that processes other than turbulence may have been acting to affect particle size.

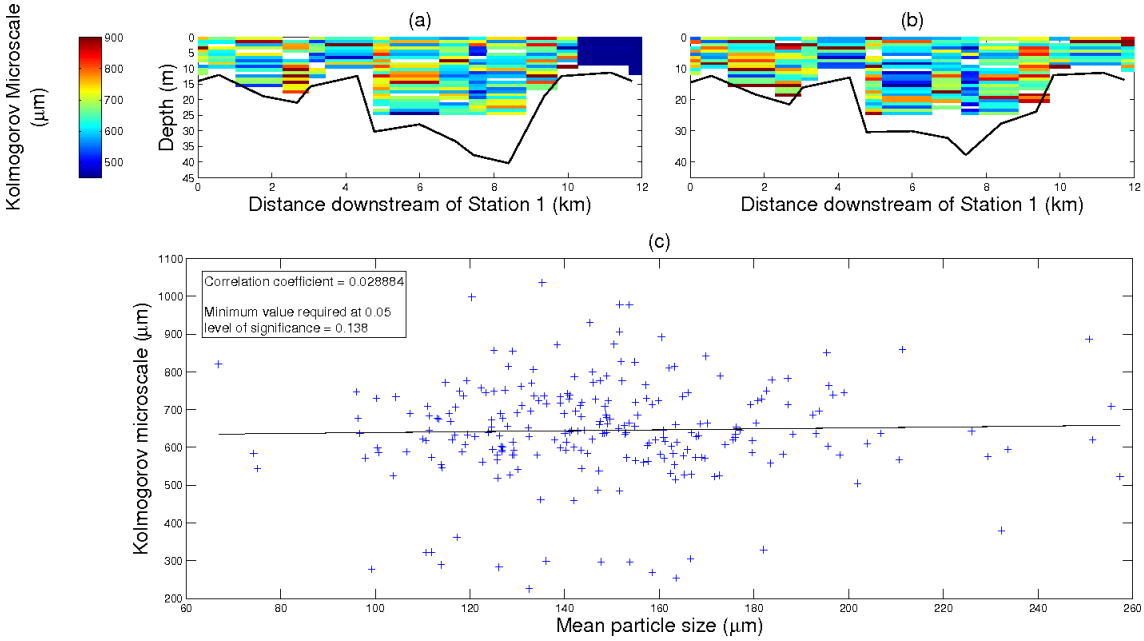

Figure 22: Kolmogorov microscales for the ebb (a) and flood (b) transects. The dark blue cells between 10.5 and 12km downstream of Station 1 in the ebb transect indicate the region where it was not possible to calculate TKE dissipation. The relationship between Kolmogorov microscale and mean particle size is shown in the scatterplot (c).

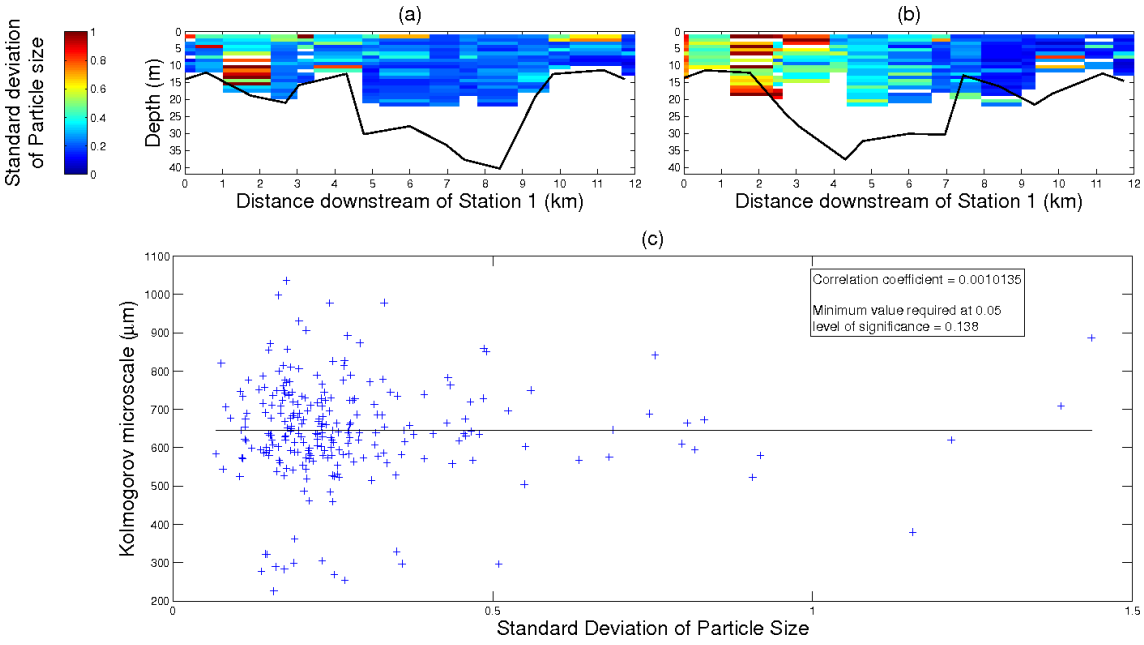

Figure 23: Standard deviation of particle size distribution for the ebb (a) and flood (b) transects. The relationship between the standard deviation of particle size distribution and the Kolmogorov microscale is shown in the scatterplot (c).

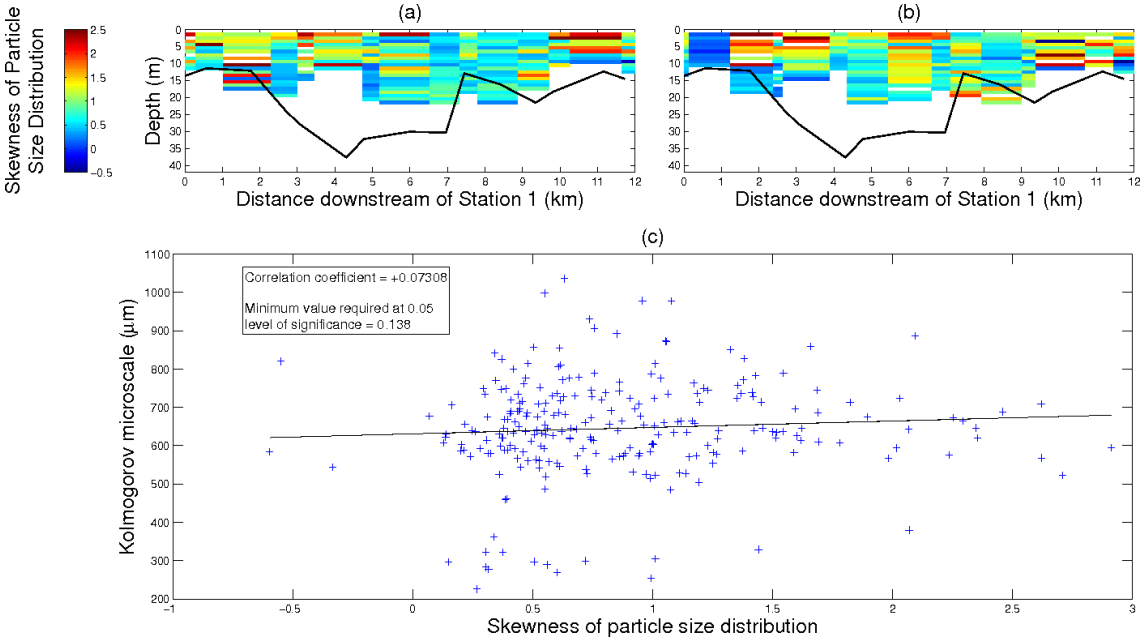

Figure 24: Skewness of particle size distribution for the ebb (a) and flood (b) transects. The relationship between the skewness of particle size distribution and Kolmogorov microscales is shown in the scatterplot (c).

A further possibility for there being no significant relationship is that the method used for determining TKE dissipation did not accurately estimate Kolmogorov microscales. This is likely to be due to the large number of errors associated with using an ADCP to measure TKE dissipation as highlighted by Wiles et al. (2006), as well as additional problems with using an ADCP on a moving boat. For example, even though the calculations were were only applied to the data when the boat was stationary for profiling, there was some variation in boat position and orientation. Any movement of the ADCP during this process would have resulted in changes to the individual beam velocities recorded, decreasing the reliability of TKE dissipation estimates. Also, the width of each acoustic beam transmitted by the ADCP increases with depth. This results in an increase in the area over which the velocities are estimated as depth increases, causing a reduction in the resolution of the velocity structure in the deeper waters. As a result, the estimation of TKE dissipation would have decreased in accuracy with depth. For a more detailed exploration into the effect of turbulence on SPM dynamics, a much higher resolution instrument, such as a profiling ADV or FLY probe, would be more appropriate.

Despite the difficulties of measuring the complex dynamics of the estuarine processes of flocculation, turbulent characteristics and their relation to the dynamics of SPM, this study has achieved the aims and objectives set out in Section 1 by identifying the influence of a number of physical processes on the distribution and size of SPM within the lower Tamar Estuary.

5 Summary and Conclusions

The suggested temperature, salinity and density structure of a partially mixed estuary made by Dyer (1997) & Uncles et al. (1986) was observed, and the hydrodynamics of the two transects made showed increased mixing during flood conditions.

Expected trends of reduced concentrations of SPM towards the mouth of the estuary (from 7mg.L^{-1} to 5mg.L^{-1}) were recorded. Acoustic backscatter highlighted some regions of high SPM concentration. However, when comparing the acoustic measurements at the surface with results obtained through the filtration of surface water samples, increased echo amplitudes were observed in locations where there was not a high concentration of SPM. This suggests that the acoustic backscatter showed response from a number of additional scatterers that were not SPM. The concentration of organic SPM was highest (2.5mg.L^{-1}) in the surface waters of the upper flood transect. Ratios of inorganic to organic SPM decreased towards the mouth during the flood tide (from 3.5 to 1.5), supporting the work of Bowers & Binding (2006).

The relationship between particle size and concentration of organic material suggests that an observed decrease in particle size towards the mouth was due to a higher concentration of organic SPM in the upper reaches of the study area. Anomalous peaks in particle size ($> 300\mu$m) identified in LISST data were often due to the presence of schlieren. The use of imaging was vital in identifying the causes of these anomalies in order for them to be removed from the analysis. A number of convoluted flocs were observed in the analysis of images obtained by digital holography. This emphasised the importance of EPS to flocculation processes, as highlighted by Dyer & Manning (1999). Particle shape is therefore an important factor to consider when characterising SPM. This suggests that the assumption of spherical particles made by LISST instruments is incorrect in locations where organic material is present.

The analysis of the data used in this study highlights the highly complex issues associated with the characterisation of SPM. Many flocs have convoluted shapes, suggesting that better shape parameterisation is required when determining particle size using instruments such as the LISST. The use of digital holography has the potential to reduce these errors and is key to identifying anomalies such as schlieren or large organisms. ADCP and OBS instruments had similar responses in conditions of high SPM concentrations (12-14mg.L^{-1}). However, they had very different responses in locations of lower SPM concentrations. It is therefore necessary for further research into the response of different instruments on a variety of different particles, using optical backscatter, acoustic backscatter and laser diffraction techniques, before an accurate characterisation of SPM can be made.

References

Admiralty (n.d.), 'Tidal stream atlas of plymouth sound'.

Agrawal, Y. C. & Pottsmith, H. C. (2000), 'Instruments for particle size and settling velocity observations in sediment transport', *Marine Geology* **168**, 89–114.

Allen, G. P., Salmon, J. C., Bassoulet, P., Perihoat, Y. D. & Grendpre, D. (1980), 'Effects of tides on mixing and suspended sediment transport in macrotidal estuaries', *Sedimentray Geology* **26**, 69–90.

Bale, A. J. (1996), '*In situ* laser optical particle sizing', *Journal of Sea Research* **36**(1), 31–36.

Bate, A. J. & Morris, A. W. (1987), '*In situ* measurements of particle size in estuarine waters', *Estuarine, Coastal and Shelf Science* **24**(2), 253–263.

Benson, T. & French, J. R. (2007), 'InSiPID: A new low-cost instrument for *in situ* particle size measurements in estuarine and coastal waters', *Journal of Sea Research* **58**, 167–188.

Bowers, G. G. & Binding, C. E. (2006), 'The optical properties of mineral suspended particles: A review and synthesis', *Estuarine, Coastal and Shelf Science* **67**, 219–230.

British-Standard (1989), 'Testing aggregates, part 103. Method for determination of particle size distribution', *Section 103.2 Sedimentation test* .

Bunt, J. A. C., Larcombe, P. & Jago, C. F. (1999), 'Quantifying the response of optical backscatter devices and tranmissometers to vartiations in suspended particulated matter', *Continental Shelf Research* **19**, 1199–1220.

Cameron, W. M. & Pritchard, D. W. (1963), 'Estuaries'. *In* Hill, M. N. (ed.), THE SEA **2,** Wiley, New York, 306-324.

Dalrymple, R. W., Zaitlin, B. A. & Boyd, R. (1992), 'Estuarine facies models: Conceptual basis and stratigraphic implications', *Journal of Sedimentary Petrology* **62**, 1130–1146.

Davies, J. L. (1964), 'A morphological approach to world shorelines', *Zeitschrift fur Geomorphologie* **8**, 127–142.

Davies, R. A. & Hayes, M. O. (1984), 'Hydrodynamics and sedimentation in wave-dominated coastal environments', **60**, 313–329. *In* Greenwood, B., Davis Jr., R. A. (ed.), *What is a Wave-Dominated Coast? Marine Geology* **60,** 313-329.

Dyer, K. R. (1997), *Estuaries: A Physical Introduction*, 2 edn, John Wiley & Sons, Chicester, West Sussex, England.

Dyer, K. R., Cornelisse, J., Dearnaley, M. P., Fennessy, M. J., Jones, S. E., Kappenberg, J., McCave, I. N., Pejrup, M., Puls, W., VanLeussen, W. & Wolfstein, K. (1996), 'A comparison of *in situ* techniques for estuarine floc setting velocity measurements', *Journal of Sea Research* **36**(1), 15–29.

Dyer, K. R. & Manning, A. J. (1999), 'Observation of the size, settling velocity and effective density of flocs, and their fractal dimensions', *Journal of Sea Research* **41**, 87–95.

Eidma, D. & Kalf, J. (1996), '*In situ* particle (floc) size measurements with the NIOZ *in situ* camera', *Journal of Sea Research* **36**(1), 49–53.

Fowler, J., Cohen, L. & Jarvis, P. (1998), *Practical Statistics for Field Biology*, second edn, John Wiley and Sons.

Fugate, D. C. & Friedrichs, C. T. (2003), 'Controls on suspended aggregate size in partially mixed estuaries', *Estuarine, Coastal and Shelf Science* **58**, 389–404.

Gentien, P., Lunven, M., Lehaitre, M. & Duvent, J. L. (1995), '*In-situ* depth profiling of particle sizes', *Deep-Sea Research I* **42**(8), 1297–1312.

Grabemann, I., Uncles, R., Krause, G. & Stephens, J. A. (1997), 'Behaviour of turbidity maxima in the Tamar (U.K.) and Weser (F.R.G.) Estuaries', *Estuarine, Coastal and Shelf Science* **45**, 235–246.

Hansen, D. V. & Rattray, M. (1966), 'New dimensions in estuary classification', *Limnology and Oceanography* **11**(3), 319.

Hill, P. S., Milligan, T. G. & Geyer, W. R. (2000), 'Controls on effective settling velocity of suspended sediment in the Eel River food plume', *Continental Shelf Research* **20**, 2095–2111.

Irigoien, X. & Castel, J. (1997), 'Light limitation and distribution of chlorophyll pigments in a highly turbid estuary: The Grionde (SW France)', *Estuarine Coastal and Shelf Science* **44**, 507–517.

Jackson, G. A., Maffione, R., Costello, D. K., Alldrdge, A. L., Bruce, E. L. & Dam, H. G. (1997), 'Particle size spectra between 1μm an 1cm at Monterey Bay determined using multiple instruments', *Deep-Sea Research I* **44**(11), 1739–1767.

Kitchener, J. A. (1972), 'Principles of action of polymeric flocculants', *British Polymer Journal* **4**(3).

Knowles, S. C. & Wells, J. T. (1996), 'Suspended aggregate analysis using ISAAC, Elbe River, 9-10 June 1993', *Journal of Sea Research* **36**(1), 69–75.

Law., D. J., Bale, A. J. & Jones, S. E. (1997), 'Adaptation of focused beam reflectance measurement to *in-situ* particle sizing in estuaries and coastal waters', *Marine Geology* **140**, 47–59.

Lynch, J. F., Irish, J. D., Sherwood, C. R. & Agrawal, Y. C. (1994), 'Determining suspended sediment particle size information from acoustical and optical backscatter measurements', *Continental Shelf Research* **14**(10/11), 1139–1165.

Maldiney, M. A. & Mouchel, J. M. (1996), '*In situ* video recording of suspended flocs', *Journal of Sea Research* **36**(1), 87–91.

Manning, A. J. & Dyer, K. R. (2002), 'The use of optics for the *in-situ* determination of flocculated mud characteristics', *Journal of Optics A: Pure and Applied Optics* **4**, S71–S81.

Mikkelesen, O., Milligan, T., Hill, P., Chant, R., Jago, C., Jones, S., Krivtsov, V. & Mitchelson-Jacob, G. (2008), 'The influence of schlieren on *in situ* optical measurements used for particle characterisation', *Limnology and Oceanography: Methods* **6**, 133–143.

Mikkelsen, O. A., Hill, P. A., Milligan, G. & Chant, R. J. (2005), '*In situ* particle size distributions and volume concentrations from a LISST-100 laser particle sizer and a digital floc camera', *Continental Shelf Research* **25**, 1959–1978.

Milligan, T. G. (1996), '*In situ* particle (floc) size measurements with the benthos 373 plankton silhouette camera', *Journal of Sea Research* **36**(1), 93–100.

Nichols, M. M. & Biggs, R. B. (1985), 'Estuaries', pp. 77–186. *In* Davies, A. A. (ed.), *Coastal Sedementary Environments*, Springer-Verlag, New York.

Nimmo-Smith, A. (2008). *Pers. com.*

O'Neill, P. (1998), *Environmental Chemistry*, third edn, Blackie Academic & Professional, London.

Perillo, G. M. E., ed. (1995), *Geomorphology and Sedimentology of Estuaries*, Elsevier.

Pritchard, D. W. (1952), 'Salinity distribution and circulation in the Chesapeake Bay', *Journal of Marine Research* **11**, 106–123.

Pritchard, D. W. (1955), 'Estuarine circulation patterns', *Proceedins of the American Society of Civil Engineers* **81**(717).

Richards, S. D., Heathershaw, A. D. & Thorne, P. D. (1996), 'The effect of suspended particulate matter on sound attenuation in seawater', *Journal of Acoustical Soc. America* **100**, 1447–1450.

Stemmann, L., Gorsky, G., Marty, J.-C., Picheral, M. & Miquel, J.-C. (2002), 'Four-year study of large-particle vertical distribution (0-1000 m) in the NW Mediterranean in relation to hydrology, phytoplankton, and vertical flux', *Deep-Sea Research II* **49**, 2143–2162.

Styles, R. (2006), 'Laboratory evaluation of the LISST in stratified fluid', *Marine Geology* **227**, 151–162.

Syvitski, J. P. M. & Hutton, E. W. H. (1996), '*In situ* characteristics of suspended particles as determined by the Floc Camera Assembly FCA', *Journal of Sea Research* **36**(1), 131–142.

Thorne, P. D. & Hanes, D. M. (2002), 'A review of acoustic measurement of small-scale sediment processes', *Continental Shelf Research* **22**, 603–632.

Thorpe, S. A. (2005), *The Turbulent Ocean*, Cambridge University Press, Cambridge.

Uncles, R. J. (1990), 'Longditudinal dispersion processes in the upper Tamar Estuary', *Estuaries* **13**(2), 118–124.

Uncles, R. J., Elliott, R. C. A. & Weston, S. A. (1985*a*), 'Lateral distributions of water, salt and sediment transport in a partly mixed estuary'. *In* Edge, B. L. (ed.), *Proceedings of the 19th Internationsl Conference on Coastal Engineering*, Chapter 204. American Society of Civil Engineers, New York.

Uncles, R. J., Elliott, R. C. A. & Weston, S. A. (1985*b*), 'Observed fluxes of water, salt and suspended sediment in a partly mixed estuary', *Estuarine, Coastal and Shelf Science* **20**, 146–168.

Uncles, R. J., Elliott, R. C. A., Weston, S. A., Pilgrim, D. A., Ackroyd, D. R., McMillan, D. J. & Lynn, N. M. (1986), 'Synoptic observations of salinity, suspended sediment and vertical current structure in a partly mixed estuary', pp. 58–70. *In* J. van Kreeke (ed.), *Lecture Notes on Coastal and Estuarine Studies*, Springer-Verlag, New York.

VanLeussen, W. & Cornelisse, J. M. (1996), 'The underwater video system VIS', *Journal of Sea Research* **36**(1), 77–81.

Wiles, P. J., Rippeth, T. P., Simpson, J. H. & Hendricks, P. J. (2006), 'A novel technique for measuring the rate of turbulent dissipation in the marine environment', *Geophysical Research Letters* **33**.

Appendix

A Tides

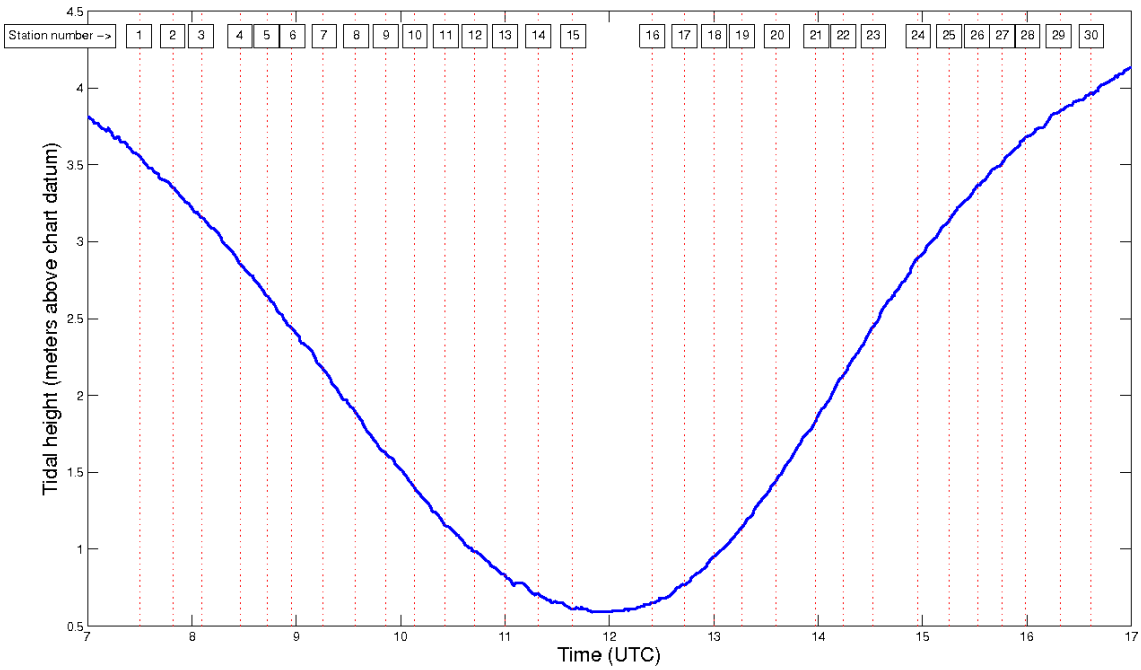

Figure 25: Tidal heights for the duration of the transects. Times for each station are marked with dotted lines.

B Meteorological Data

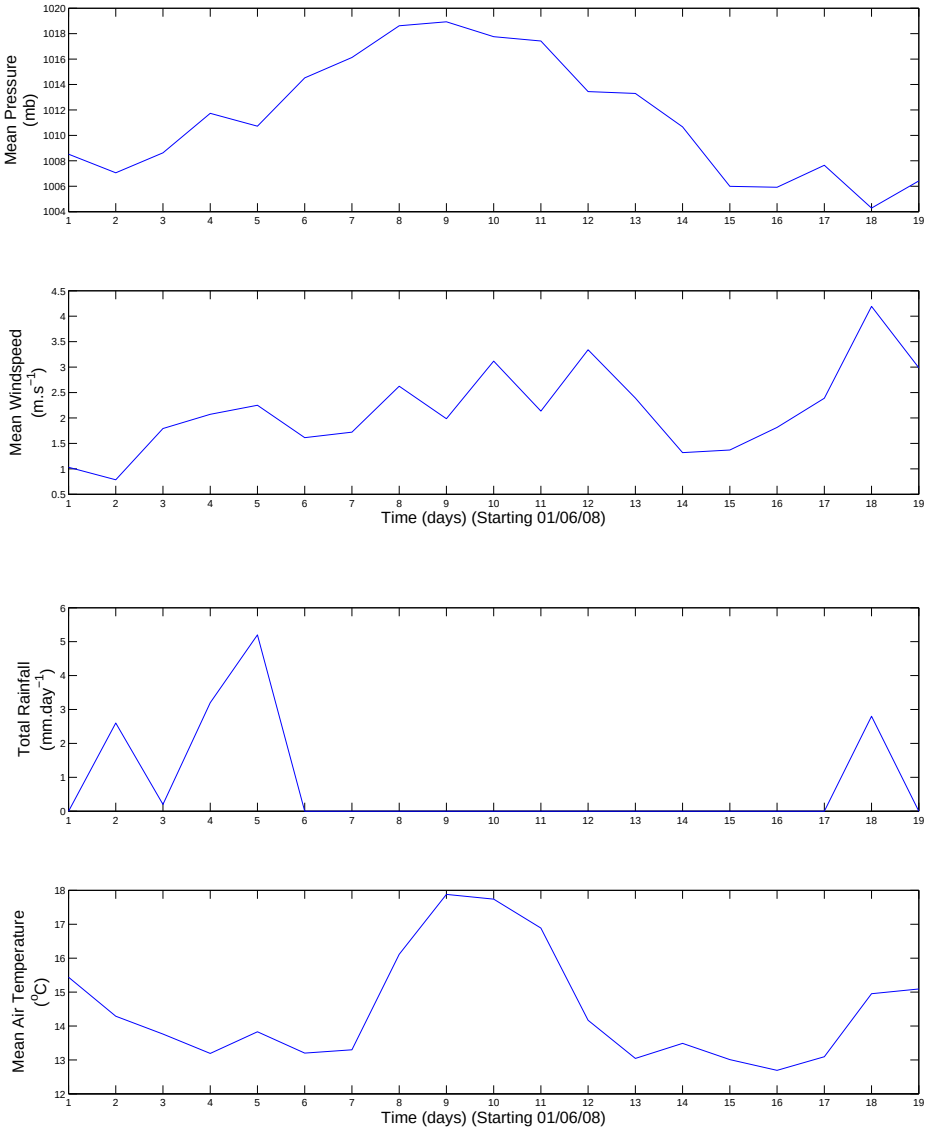

Figure 26: Meteorological data leading up to the time of data collection. (Obtained from the Fitzroy weather station on the University of Plymouth campus.)

Figure 26 shows that the period between the 15th and 19th of June consisted of relatively low atmospheric pressure and high mean windspeeds. There was very little rain during the days preceding the data collection, other than between the 1st and 6th of June and during the 18th June.

C Calibration of OBS & Fluorometer

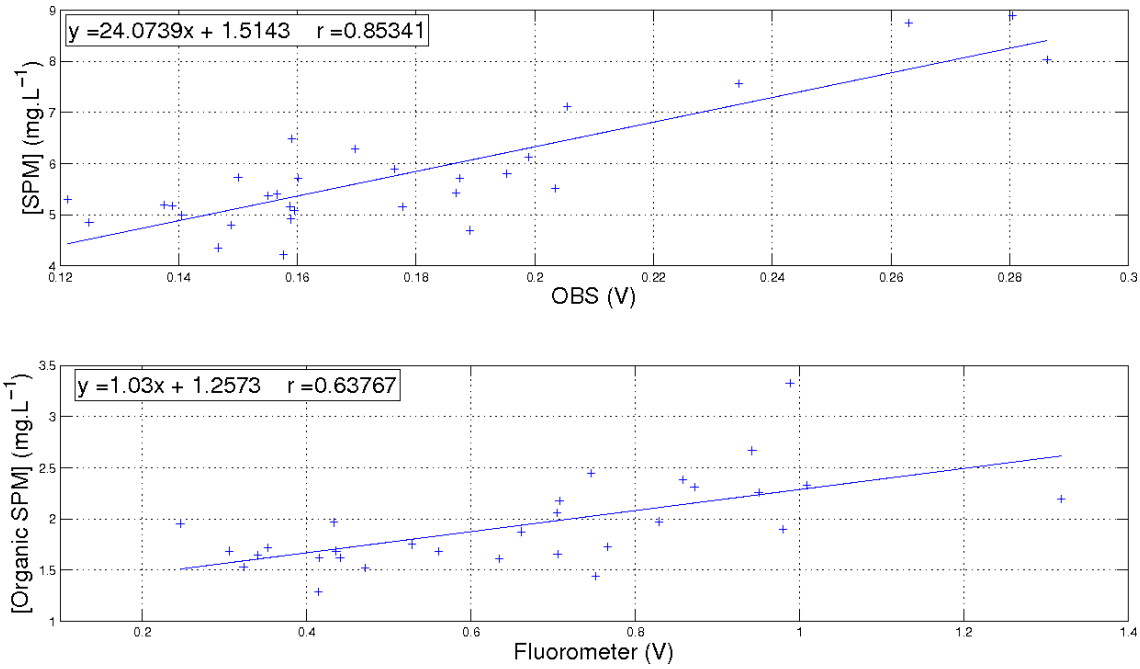

Figure 27: The relationship between SPM concentrations obtained through filtration and the OBS & Fluorometer response at a depth of 2m.

Product moment correlation coefficient:

$$r = \frac{n\Sigma xy - \Sigma x \Sigma y}{\sqrt{[n\Sigma x^2 - (\Sigma x)^2][n\Sigma y^2 - (\Sigma y)^2]}}$$

OBS:

$$\begin{aligned} \Sigma x &= 5.3291 & \Sigma y &= 173.7204 \\ (\Sigma x)^2 &= 28.3991 & (\Sigma y)^2 &= 30179 \\ \Sigma x^2 &= 0.9982 & \Sigma y^2 &= 1047 \\ n &= 30 & \Sigma xy &= 32.0992 \end{aligned}$$

$$\begin{aligned} r &= \frac{30 \times 32.0992 - 5.3291 \times 173.7204}{\sqrt{[30 \times 1047 - 30179][30 \times 0.9982 - 28.3991]}} \\ r &= 0.8534 \\ 0.8534 &= \text{A strong correlation} \end{aligned}$$

Fluorometer:

$$\begin{aligned} \Sigma x &= 19.697 & \Sigma y &= 58.0058 \\ (\Sigma x)^2 &= 387.9726 & (\Sigma y)^2 &= 3364.7 \\ \Sigma x^2 &= 14.9461 & \Sigma y^2 &= 117.4092 \\ n &= 30 & \Sigma xy &= 40.1588 \end{aligned}$$

$$\begin{aligned} r &= \frac{30 \times 40.1588 - 19.697 \times 58.0058}{\sqrt{[30 \times 14.9461 - 387.9726][30 \times 117.4092 - 3364.7]}} \\ r &= 0.6377 \\ 0.6377 &= \text{A modest correlation} \end{aligned}$$

The calculated correlation coefficients of 0.8534 and 0.6377 (calculated above) exceed the tabulated value in Appendix 5 of Practical Statistics for Field Biology (Fowler et al. 1998) at 28 degrees of freedom, of 0.361 at a 0.05 level of significance. Both correlations are therefore statistically significant and the following equation can therefore be used to calibrate the OBS and Fluorometer from the filtration results:

$$y = mx + c$$

OBS calibration:

$$\begin{aligned} y &= mx + c \\ SPM_{OBS} &= 24.0739 \times Voltage_{OBS} + 1.5143 \end{aligned}$$

Fluorometer calibration:

$$\begin{aligned} y &= mx + c \\ OrganicSPM_{Fluorometer} &= 1.03 \times Voltage_{Filtration} + 1.2573 \end{aligned}$$

These formulae were applied to all the OBS and Fluorometer data.

D Calibration of ADCP Backscatter

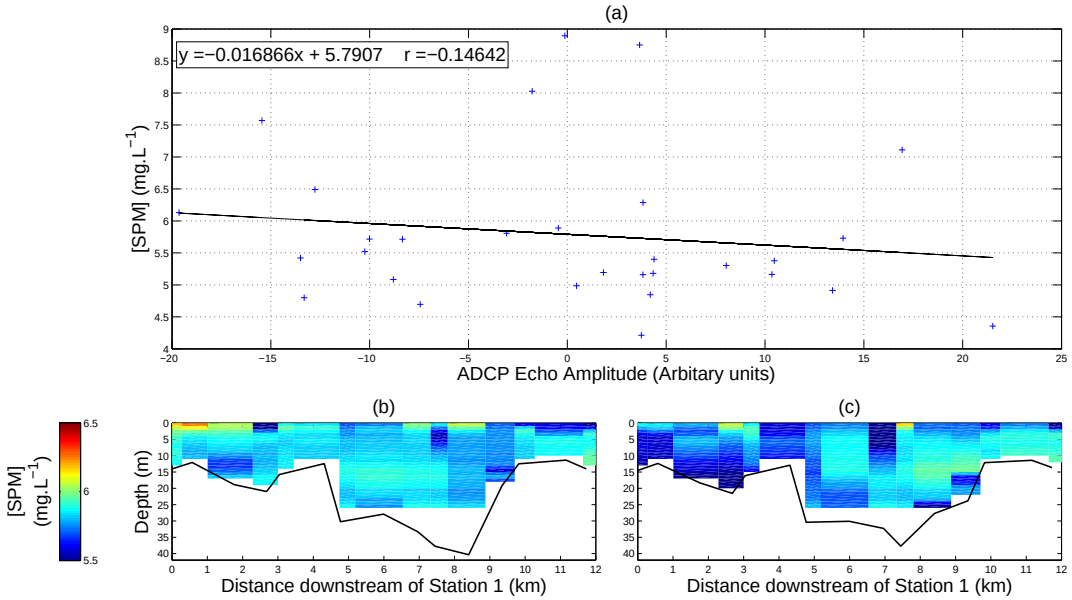

Figure 28: The relationship between SPM concentrations obtained through filtration and the ADCP echo amplitude at a depth of 2m (a). Calibrated ADCP echo amplitudes for the ebb (b) and flood (c) transects.

The same method of calibration used in Appendix C was used. It is clear that this calibration was not successful due to there being no relationship between surface SPM concentration and the ADCP echo amplitude at 2m.

E ADCP Current Velocities

E.1 Station Timing Check

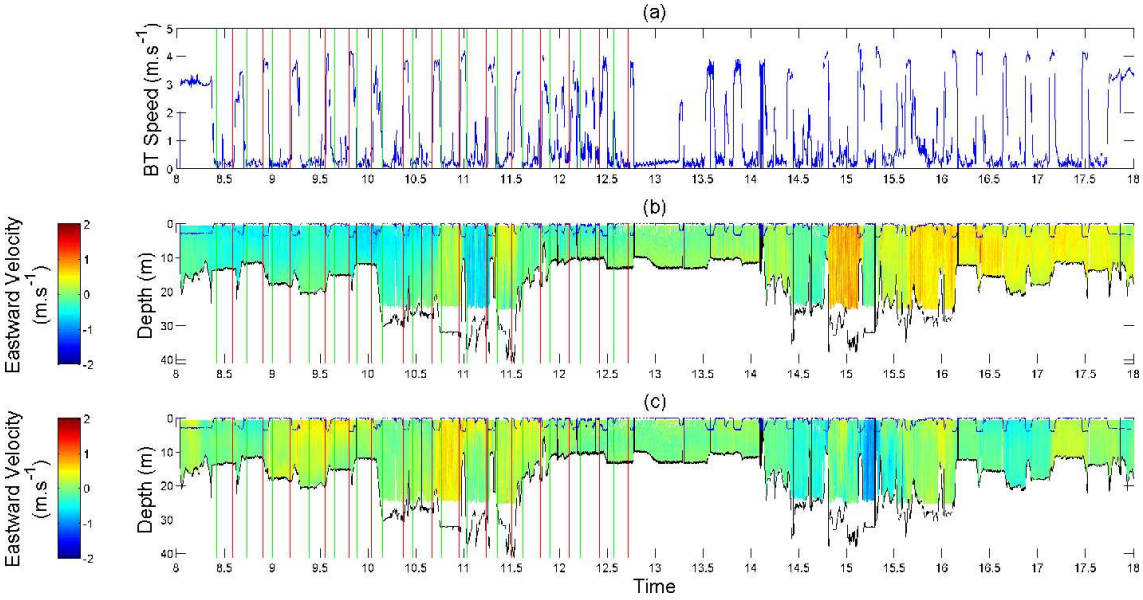

Figure 29: Comparison between bottom tracking speed and the start times (green lines) and finish times (red lines) at each station (a).

It is clear from graphs (b) and (c) of Figure 29, that bottom tracking depths (black line) and current velocities were roughly constant between the green and red lines. This confirms that the timings were accurate and that the data between green and red lines could be averaged to produce time-averaged velocities for each station.

E.2 ADCP Current Velocities Before Rotation

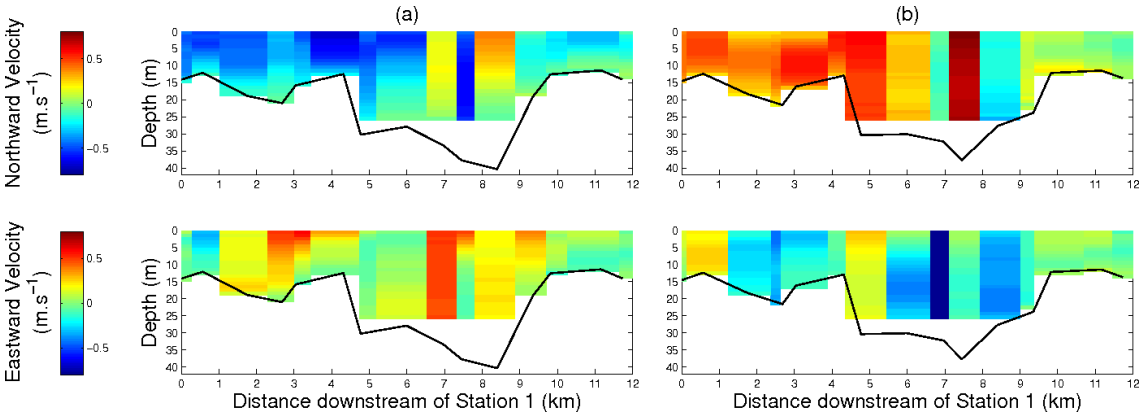

Figure 30: Northward and Eastward ADCP current velocities recorded on the ebb (a) and flood (b) transects.